Assessment of Colloidal Self-Assembly for Photonic Crystal
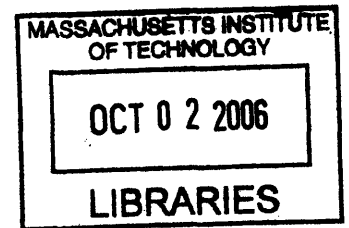
by

Chan Hoe Yip

B. E. Electrical and Electronic Engineering
Nanyang Technological University, 2001

SUBMITTED TO THE DEPARTMENT OF MATERIALS SCIENCE AND
ENGINEERING IN PARTIAL FULFILLMENT THE REQUIRMENTS FOR THE
DEGREE OF

MASTER OF ENGINEERING IN MATERIALS SCIENCE AND ENGINEERING
AT THE
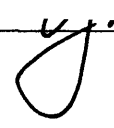MASSACHUSETTS INSTITUE OF TECHNOLOGY

SEPTEMBER 2006

Signature of Author:

Department of Materials Science and Engineering
August 10, 2006

Certified by:

Yet-Ming Chiang
Thesis Supervisor
Kyocera Professor of Ceramics

Accepted by:

Samuel M. Allen
POSCO Professor of Physical Metallurgy
Chair, Departmental Committee for Graduate Students

Assessment of Colloidal Self-Assembly for Photonic Crystal

by

Chan Hoe Yip

Submitted to the Department of Materials Science and
Engineering on August 10, 2006 in Partial Fulfillment of the
Requirements for the Degree of Master of Engineering in
Materials Science and Engineering

Abstract

A suspension of monodisperse colloids has an interesting property of self-assembling into a three-dimensional ordered structure. This crystalline material has attracted significant interest on the implementation of photonic crystals, which have practical applications in reflectors, filters, resonators, and waveguides. In this thesis, self-assembly of colloidal crystals and photonic crystal technologies are reviewed. Potential colloidal photonic and non-photonic devices were presented and their values/limitations were discussed. Colloidal photonic crystals were assessed on their technical capabilities, growth techniques and fabrication cost.

In this assessment, the bulk colloidal photonic crystals are found to be inherently robust against stacking disorder, cracks and voids. The high reflectance performance and lattice parameter tailoring are useful for implementing reflectors, optical switch and sensors. Besides, the anomalous dispersion characteristic near to the band edges or near to flat bands of the photonic band diagram is suited for superprism and light harvesting applications. Potentially, the unique characteristics of colloidal photonic crystal could be capitalized in a low cost micro-fabrication model. Finally, the study has shown that it is more technically and commercially viable to implement bulk colloidal photonic crystal applications rather than lithographically-defined types.

Thesis Supervisor : Yet-Ming Chiang
Title : Kyocera Professor of Ceramics

3

Blank Page

Acknowledgement

I would like to thank my advisors Professor Yet-Ming Chiang and Associate Professor Chee Cheong Wong (Singapore-MIT Alliance, Nanyang Technological University) for their guidance, support and encouragement throughout the course of my research.

I am grateful to Singapore-MIT Alliance (SMA) for their financial support and administration assistance towards my studies, which uniquely span across MIT and Singapore campuses. I am indebted to Jocelyn, John and Andrew (SMA-MIT) for helping me to settle in MIT and their sincere care rendered across the Pacific Ocean while I am at Singapore. I must thank Vino, Juliana and Associate Professor Choi (SMA-Singapore) for their kind support.

I am appreciative of my colleagues in Associate Professor Wong's Colloidal Group at Nanyang Technological Univeristy, Singapore. Yaw Koon has been patient and great while sharing me his knowledge. Lay Kuan has been feeding me cost data information for the preparation of the cost analysis. I have several fruitful discussions with Dr Yan. Thanks. Kwan Wee offered to help me to correct mistakes in my thesis. Xiaofang and the whole group were kind to take time off to attend my mock final presentation.

I enjoyed the M.Eng course because of the wonderful classmates around. Foo Nun, Kah Pin, Jonathon, Jing Wei, Johnathan, Zou Ting, Kelvin, Xiao Dong, Xin Yue, Guo Qiang, Wang Miao, Fatwa, Hashina and Raj are fun people to work with. Professor Kimerling and Dr Saini (3.46 course instructors) were instrumental in helping me to explore the world of micro-photonic.

Finally, I like to express my gratitude to my wife, Candy, and my family for their cheering whenever I am feeling down. They have been very understanding to me as we have to forgo vacations and weekends during my studies.

Thank you.
- Chan Hoe -

Content

1.0 Introduction

In the pursuit for nano-scale microelectronic devices, the current microelectronics capabilities are nearing to the limits. The need for speed and low-power consumption in portable devices hastens the pace of device scaling. Microelectronics is approaching into a phase where minimum features are only hundreds of atoms wide. Radical and disruptive technologies are essential to meet future challenges. Today, the focus has shifted to advanced material engineering, for instance on developing silicon-germanium (SiGe) compound for Heterojunction Bipolar Transistor (HBT) technology[1]. Without pushing the limit of physics with device scaling, the use of the relatively more expensive SiGe material allows smaller, cheaper and faster integrated chips to be implemented.

Self-assembly or self-organization technique, on the other hand, holds great potentials to meet the challenges for alternative fabrication technologies[2]. In a self-assembly process, building blocks configure themselves to generate a myriad of structures in materials[3]. Nature has participated in the spontaneous formation of material with ordered structures. Building blocks, such as atom, molecules and colloidal particles define the uniqueness properties of materials by the way how these building blocks are arranged. For example, carbon atoms arranged in diamond-structure or graphite-structure has vastly different hardness property.

Interestingly, the self-assembly technique is anticipated to create huge impact on nano-fabrication in a revolutionary way: nano-scale components could be brought together and assembled by just stirring the solution[4]. This self-assembly method could find applications in building microelectronic device and biology cell. Self-assembly is ubiquitous in chemistry and biology, however it is relatively untapped in micro-fabrication[5]. It offers attractive opportunities in handling minuscule building blocks not possible by today's technologies while simplifying processing and lowering cost.

Self-assembly of sub-micron monodisperse colloidal particles such as polystyrene (PS) or silica microspheres into ordered structures have attracted intense interest due to its potential for forming intricate structures with geometries or scale not able to achieve with present fabrication techniques. The engineering of the structure of the colloidal crystal can be served as a template for photonic devices and humidity/pH/glucose sensors.
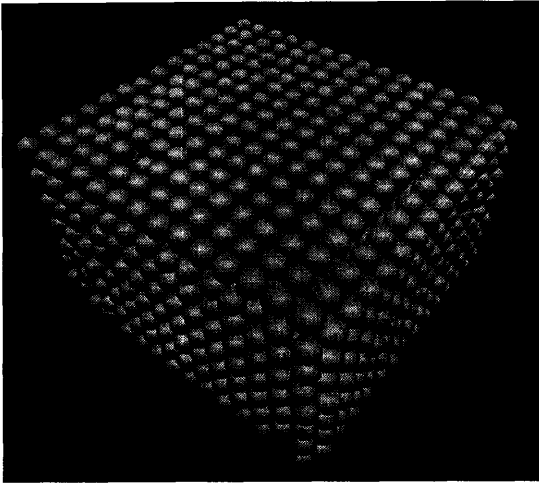
Figure 1. A FCC colloidal crystal with microspheres and air voids. This serves as an infiltration template to implement a photonic crystal. Picture source: Bell Lab.

1.1 Background

In the age of maturing micro-fabrication, the future entails a radical change in processing and thinking. Today, hybrid or even fuel-cell automobiles are poised to be the next major research effort in light of rising oil price. Further, semiconductor companies like Intel, which thrived on device-scaling in the past, has make a revolutionary move to dual-core microprocessor chips for personal computer. Looking in the future, there is a great challenge to deliver more data faster. People will be downloading full-length movies at home, on top of digital photos and music files. To meet the projected demand on speed and bandwidth, IBM and Intel are exploring the use of light to transmit data. Using materials like Silicon Photonics[6] or Photonic Crystal[7] in replacement of the mainstream semiconductor devices, light signal can be manipulated efficiently and transmitted over longer distance.

Numerous micro-fabrication techniques are currently pursued by many research groups[8] around the world for photonic crystal materials. In this thesis, self-assembly method for photonic crystal using colloidal particles is discussed. As an outline for the complete colloidal crystallization process, monodisperse colloidal particles (e.g. polymer or silica microspheres) in aqueous suspension are allowed to assemble spontaneously to form a colloidal crystal. This colloidal crystal is then infiltrated with a high dielectric material such as silicon and the colloidal microspheres are removed subsequently by

9

calcinations or chemical etch. As a result, an inverse opal (air spheres and silicon filling in the interstitial) is obtained. This structure presents a photonic bandgap and is called the photonic crystal.

1.2 Scope of Thesis

The self-assembly of colloidal crystal is reviewed and investigated for the implementation of photonic crystal based on existing fabrication techniques in chapter 2 and 3. Several case studies on colloidal photonic crystal research are presented and analyzed in chapter 4. Limitations on colloidal photonic crystal implementation are also discussed. Potential applications are outlined. Finally, a cost analysis of fabrication is conducted to assess commercial viability and cost optimization in chapter 5.

2.0 Photonic Crystal

Photonic crystal, a promising new class of material, was reported to have proven long-standing theory to manipulate light in an issue of Science Journal 1998[9,10]. MIT researchers had managed to control the flow of light using Photonic Crystals. They were able to guide light around a 90-degree turn with high efficiency. This was a small step but an enabling technique of molding and guiding light could lead to many novel photonic applications.

Since 1970s, light transport is the key for optical telecommunication, which is widely used for transmitting data for Internet and telephone over long distances. Transmitting in the speed of light and having no electric charges unlike electrical signal, light can send much more information through optical fibers than electrical signals through wires. Further, advances in refining impurities for optical fiber enable long range and low loss optical telecommunication.

On a micro-scale, photonic crystal has the potential to be the material to integrate all the myriad functions found in an optical network system. With the goal of implementing waveguides, switches and modulators using photonic crystals, a single chip of Photonic Integrated Circuit (PIC) could be developed. This has a great commercial potential to replace all bulky and costly optical components.

Photonic crystals have macroscopic structures consisting of periodic variation of the dielectric material. Using a suitable structure, the photonic crystals can present photonic bandgap (similar to the electronic bandgap theory), for the prohibition of photons propagation.

Using the analogy of nearly free electrons model in a semiconductor, one could understand the behavior of propagation of light in a photonic crystal. For example, a diamond-lattice structure of silicon material, presents a periodic potential to the free electrons moving through. Using Quantum Mechanics theory, the columbic interaction between the periodic potential and the electrons gives rise to the formation of allowed and

forbidden energy states, collectively know as energy bands. At room temperature, silicon has a forbidden energy bandgap, approximately 1.1 eV, where electrons cannot be found.

In a photonic crystal, photons moving through this material intersperses with regions of high refractive index and low refractive index. To a photon, this refractive index contrast looks just like the periodic potential that an electron experiences traveling through a silicon crystal example. Light entering the composite material will reflect through and partially reflect off the myriad internal interfaces of high and low refractive index materials. P erfect c ancellation i n a ll d irections f or a b and o f w avelength g ives r ise t o a complete photonic bandgap. The larger the contrast of refractive indices, the wider is the photonic bandgap . Joannopoulos' text[11] provides a rigorous treatment of photonic crystal physics.

The periodic structure of a photonic crystal can be thought of a regular arrangement of scattering centers for light. There can be some structures which could present scattering centers for a particular electromagnetic wavelength (wave cancellation from refraction and reflection in scattering centers). This can occur if the dimension of the periodicity is on the order of wavelength of light. The crystal will block light with wavelengths within its photonic bandgap, while allowing other wavelengths to pass freely. A complete photonic bandgap is formed if light is forbidden to enter the photonic crystal no matter which direction the light is coming from.

The strong point of photonic crystals is the flexibility in controlling the width and spectral position of the gap through (i) varying the refractive constant of the materials and, (ii) the dimension of the periodicity of the dielectric materials. Hence, the optical property can be tailor to prohibit the propagation of light, make mirror out of wave reflection. On top of it, the photonic crystal can be functionalized into an application-specific device such as: introducing a point defeat to make a micro-cavity or a line defect to make a waveguide structure.

Examples of naturally occurring photonic crystals are opal stones and the feather of a peacock as depicted in figure 2. These materials contain special arrangement of dielectric materials a nd a ble t o r eflect o ff b rilliant h ue o f l ight (photonic b andgap i n v isible l ight region). A closer look on the feather's surface using scanning electron microscopy (SEM)

reveals the ordering of dielectric spheres with air filling (see figure 2(b), insert). This presents a photonic bandgap for frequencies corresponding to the dimension of the spheres periodicity. Hence, a multiple colors of peacock's feather can be seen.
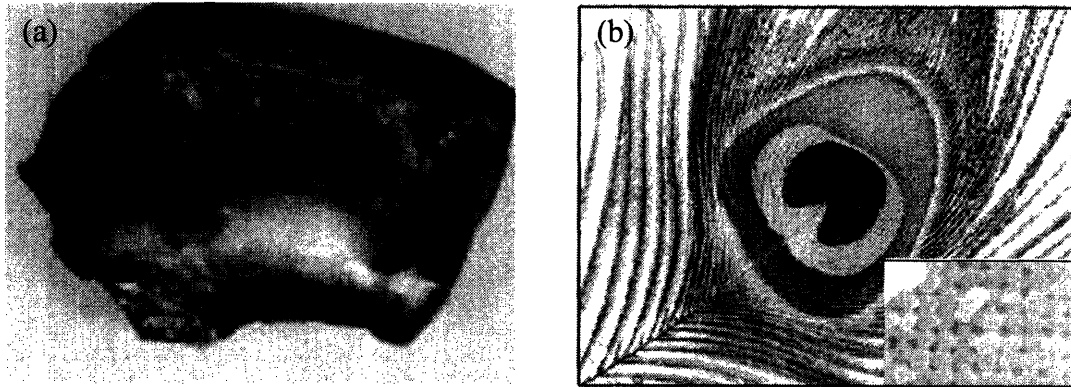

Figure 2. Naturally occurring photonic crystals (a) opal stone and (b) feather of a peacock.

2.1 The Development on Photonic Crystal

In 1946, Purcell[12] published a short note on how the radiation rate of photons from an excited atom can be controlled by modifying the space that surround the atom. By having a small volume of engineered material, the spontaneous emission rate can be inhibited. The density of states is suppressed and the excited carriers are not able to de-excite into photons. Hence, spontaneous emission is suppressed. This may be the original idea on how the periodic dielectric variation in a material could have an influence on the electromagnetic wave passing through. In 1979, Ohtaka[13] made a study of scattering effects and reflection of electromagnetic field through an arrayed of dielectric cylinders. These early researches, among others, started off the pursue of photonic bandgap structure.

The research effort on a photonic bandgap probably peaked during the late 80's with two prominent teams led by Eli Yablonovitch (Bell Communications Research) and Sajeev John (Princeton University)[14]. They believed that a bandgap could be created for photons in the same way that a semiconductor possesses an electronic bandgap. Then, the two teams met and coined the terminology 'Photonic bandgap'. However, both teams clearly had different perspectives on photonic bandgap. John et al was interested into light localization studies in a disordered material, while Yablonovitch et al pursued on the equivalent electronic bandgap for light. Moving on, Yablonovitch et al[15,16] proposed and demonstrated the existence of a 3D photonic crystal in a Yablonovite[14] structure (figure 3). Calling their photonic crystal as the 'semiconductor of light', the Yablonovite structure had 500,000 holes painstakingly drilled onto the dielectric plate and didn't look much of a potential commercial product then.

A relatively less tedious method of fabricating the photonic crystals structure, called woodpile photonic crystal, was introduced by Ho et al[17] in 1994. The woodpile photonic crystal structure consisted of layers of dielectric rods of circular, elliptical, or rectangular shape, as shown in figure 4(a). It involved a combinational of various microelectronic techniques namely: layer-by-layer film growth, chemical-mechanical polishing (CMP) and etching[18]. It is one of the most popular 3D lattices and provides great

flexibility for the design of a photonic crystal structure with a large photonic band gap at a given dielectric contrast[14].
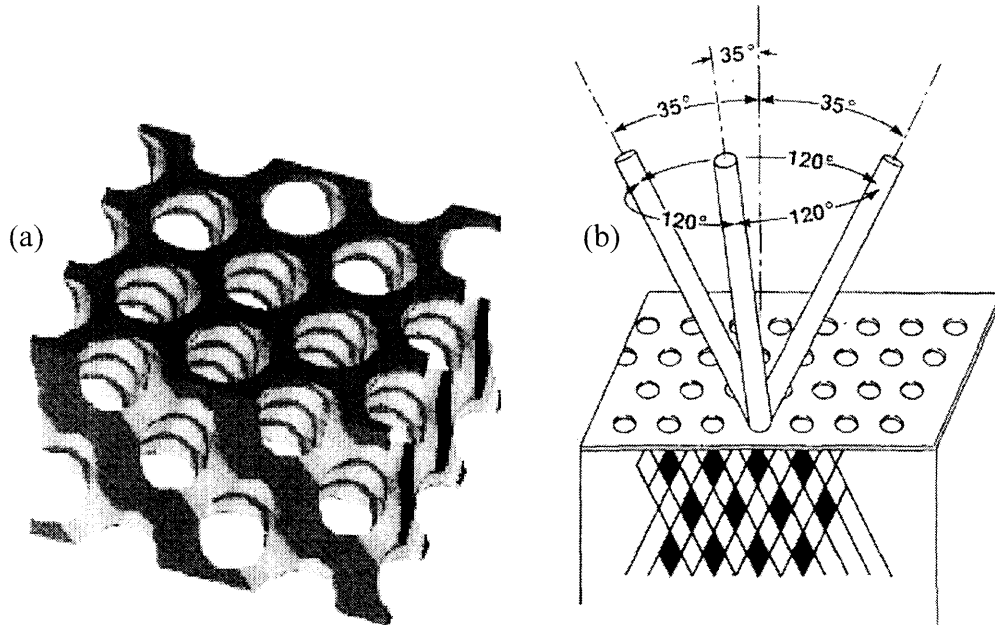
Figure 3. (a)   Yablonovite Structure. (b) Each hole is drilled through three times at an angle 35.260 away from normal and spread 1200 on the azimuth. The drilling can be done by a real drill bit for or by reactive ion etching.

Figure 4(b) shows a colloidal inverse opal structure (Face centered cubic, FCC, structure with dielectric fillings and air holes) with a photonic bandgap. The inverse opal needs a high refractive index (n > 2.8) material to allow a complete photonic bandgap to form in the 8th and 9th bands. Silicon is the best suitable material to build a photonic crystal because it has a high refractive index (n = 3.5). In 2000, a demonstration of inverse opals was performed using colloidal crystal[19]. A FCC lattice of close packed mono-dispersed silica spheres was assembled[20] and this formed the template for silicon infiltration. The void lattice of opal was infiltrated silicon under low-pressure chemical vapour deposition (LPCVD)[21]. After infiltration, the silica template was removed by wet etching and an inverse opal structure was attained.

Ho et al[22] observed that dielectric spheres arranged in diamond structure do possess a full photonic bandgap. In their studies, they concluded that an even lower refractive index contrast (n ~ 2) was needed to open up a gap. Compared with the previous inverse opals, the photonic bandgap of the diamond structure is much wider and more robust[22]. The findings opened up a new quest for the methods to obtain a diamond structure. Figure 4(c) shows the arrangement of dielectric spheres in diamond structure. To date, the fabrication of a diamond structure is still at its research phase. There are reports on the used nano-robotic arm to pick the dielectric spheres and construct them into a diamond structure[23].
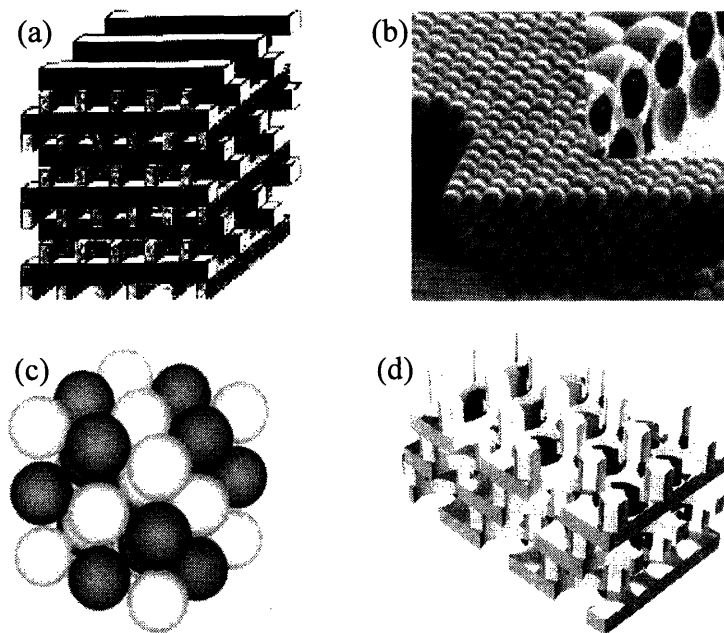
Figure 4. Examples of photonic crystal structures. (a) woodpile, (b) colloidal crystal, insert: inverse opal structure, (c) dielectric spheres arranged in diamond structure , (d) MIT Photonic Crystal.

Figure 4(d) shows another photonic crystals structure[24], commonly knows as MIT Photonic Crystal in the research fraternity. In 2000, Johnson and Joannopoulos introduced a structure of alternating stack 2D slabs consisting of dielectric rods in air and air holes in

dielectric. They made used of lithographic/etch technique and layer-by-layer fabrication technique. This structure has a wide complete bandgap for Silicon/air system, and it even demonstrated a fairly wide bandgap for the moderate Si/SiO_2 refractive index contrast.

2.2 The Future for Photonic Crystal

Since the invention of the laser and optics fibers, optical communication has revolutionized the world on how high-speed data rate can be achieved over great distance. Today, photonic crystals technology paves the paradigm shift towards information processing on a micro-scale (figure 5). Around the world, photonic crystal technology is An upcoming research area[25], where more novel functions using photonic crystal material could be unraveled.
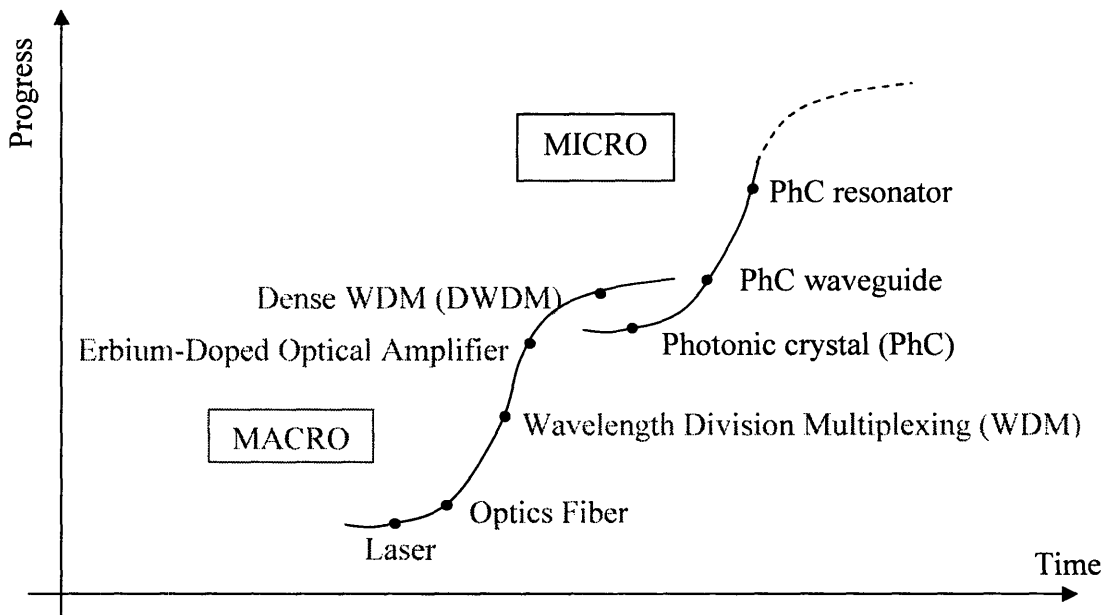
Figure 5. A paradigm shift: macro to micro optical system.

Joannopoulos Research Group[26] of MIT envisioned the Photonic Micropolis shown in figure 5(a). It is an idealized depiction of a "photonic micropolis" incorporating many functional blocks of an optical system. The highways and bridges mimicked waveguides

for light. The tall buildings represent active devices such as switches and modulators for light. The vision is to develop a Photonic Integrated Circuit (PIC) as shown in figure 6. PIC should incorporate many of the basic function found in an optical system, i.e. waveguides, signal switches, modulators, filters, resonators and lasers.

(a)

Waveguide	Signal Switches

Multiplexer / De-Multiplexer	Cavity Resonator / Modulator
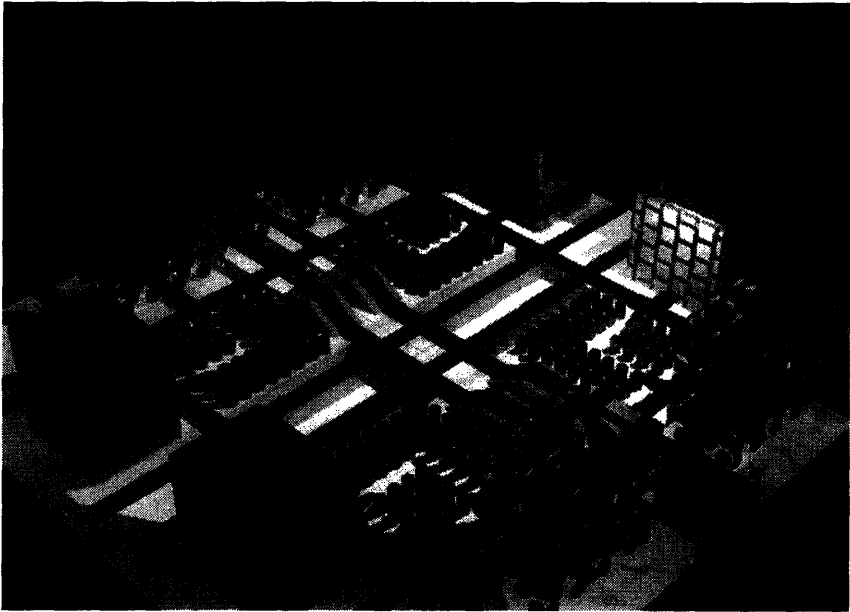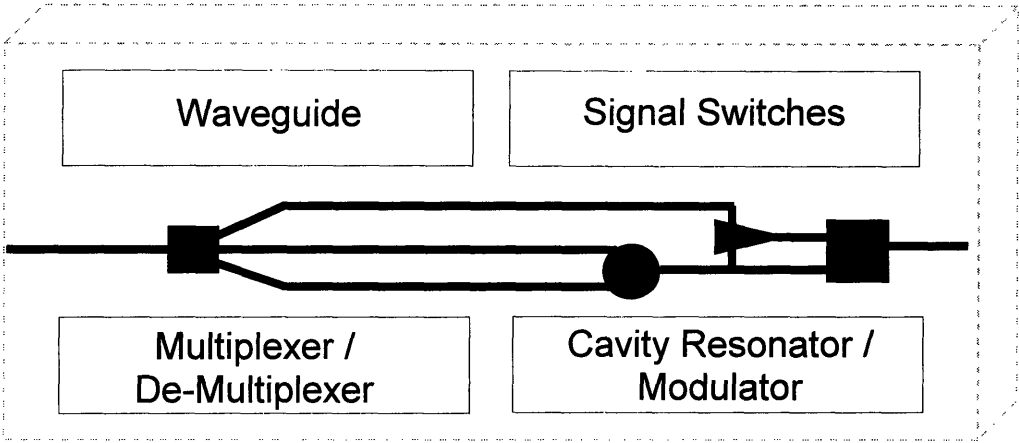
(b)

Figure 6. (a) A vision : Photonic Micropolis, (b) a photonic integrated circuit packed with basic light manipulation functions.

18

2.3 Fabrication Techniques of Photonic Crystal

The fabrication of a photonic crystal was first demonstrated by Yablonovitch et al with a 3D Yablonovite structure shown in figure 3. Using a large dielectric plate and drilling machine, the structure was made in a mechanical workshop. Their structure was tested to have a photonic bandgap in the vicinity of microwave frequency due to its relatively large air hole spacing.

To design a photonic crystal in range of visible light spectrum, the dielectric spacing has to go even smaller length. Silicon was found to be most suitable material to implement on during the infancy of the research because of availability of lithography to make small pattern on silicon and its high refractive index. The high refractive index of silicon could potentially pair with other material or air to give a high refractive index contrast photonic crystal. Hence, it can result in a complete and a wide photonic bandgap. Since then, the fabrication of the photonic crystals is largely carried out in microelectronic laboratories. Today, there are two main methods in the fabrication of photonic crystals, i.e. micro-fabrication and colloidal self-assembly methods.

(a)   (b)
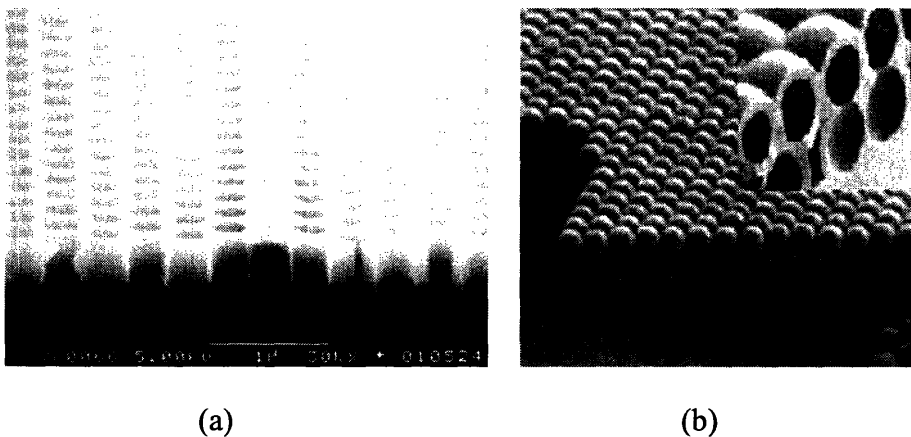
Figure 7. Microelectronic fabrication technique: 2D waveguide structure on slab, (b) colloidal self-assembly method, insert: inverted opal structure.

The micro-fabrication or "top-down" method uses the microelectronic fabrication in the making of 3D Woodpile structure in figure 4(a). The photonic crystal is fabricated

19

by using micro-fabrication patterning and etching techniques. The optical properties of these micro-structures will be characterized and studied using optical measurement techniques. In the case of 1D photonic crystal, alternating layers of varying dielectric materials were grown to create a dielectric mirror, popularly known as the Bragg's reflector. For a advanced 2D waveguide structure on slab in figure 7(a), a film is deposited onto the silicon and the pattern is transferred using lithography. Finally etching is carried out to create the air holes. The top-down method, as the name suggests, create patterns after the material is grown and it is compatible with standard semiconductor processing techniques.

(a)

(b)

(c)

(d)
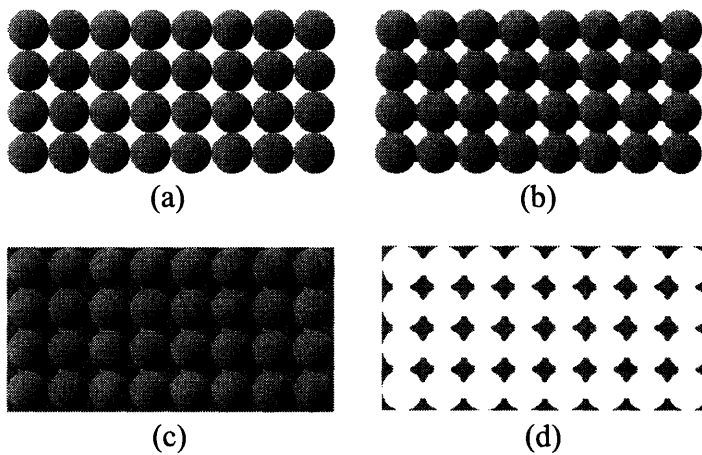
Figure 8. Steps in the formation of an inverse opal structure. (a) Colloidal Crystallization, (b) Sintering, (c) Infiltration, (d) Calcination.

The colloidal self-assembly method is a new technique to address the higher cost of the microelectronic technique. In the "bottom-up" colloidal self-assembly, colloidal spheres, such as polystyrene (PS), polymethylmethacrylate (PMMA) or silica, are suspended in solution and allow to self-assembly into colloidal crystal. Figure 7(b) shows the synthetic opal arrange in a closed packed FCC structure with air voids. Under sedimentation or capillary force, these spheres are packed into a FCC structure in its dry form and can be used as a template for making photonic crystal. The synthetic opal is next sintered prior to infiltration, depicted in figure 8(a). Sintering of opal creates the necking amongst the micro-spheres and provides added mechanical strength to the structure[27]. It also provides the inter-sphere links between the micro-spheres, which can be easily removed by chemical etching after infiltration[28]. However, too much sintering causes the reduction in solid-to-air ratio of the inverse opal and hence the photonic bandgap suffers[29].

These voids in the synthetic opal are then infiltrated with a high dielectric material using electrodeposition or CVD. Finally the colloidal spheres are removed using chemical etching or high temperature annealing, resulting in an inverted opal structure. This inverted opal structure was shown to have a photonic bangap. This colloidal self-assembly method is currently in research phase and shown to be less costly and is a less tedious approach. To date, templated-assisted[30] and electric field-assisted methods[31] were studied to better control the colloidal crystal growth.

.

3.0 Colloidal Self-assembly Techniques for Ordered Structures

As discussed previously, the natural assembly of colloidal monodisperse microspheres is potentially a simpler and cheaper approach for creating three-dimensional periodic structures[32]. Under gravitation sedimentation[33] or vertical deposition[34], colloidal self-assembly tends to form a colloidal crystal (FCC structure) spontaneously, which served as a template for photonic crystal. Besides, application specific devices can be created out of a colloidal crystal by incorporating extrinsic defects. If an intrinsic or extrinsic defect is present in the periodic structure, localized photonic states in the photonic bandgap will be created. A point defect is like a microcavity (traps light and builds up in intensity), a line defect is like a waveguide, a planar defect introduces passband in the bandgap. To incorporate a defect[35] or to fabricate a unique crystalline structure, colloidal self-assembly can be aided by templating[36], electrophoresis[37], Ionic Colloidal Crystallization[38] or lithography/etch. All these techniques are discussed in the following sections.

3.1 Colloidal Particles

An exciting area of application of colloidal particles is that of photonic bandgap materials. Colloids are particles of wide range of sizes, typically between 1 nm and 100μm. For photonic application, the sizes of interest are within ~100nm to ~1um range, which corresponds to between visible light to near-infrared spectral. Some examples of colloids are polymer (PS and PMMA), silica, silver halide and gold[39]. A colloidal suspension is described as solid particles that are dispersed in a liquid, while on the other hand; emulsion and foam are liquid particles and gas particles dispersed in a liquid respectively. Monodispersed colloid particles are commonly synthesized through emulsion polymerization for polymer microshpheres (polystyrene) and controlled precipitation for inorganic oxide microspheres (silica).

Colloids are very fine particles whose surface forces overcome its body forces. A colloidal particle consists of electric double-layers at the surface: the inner compact layer

and the outer diffuse layer [40]. During the synthesis, the surfaces are often terminated with end groups such as: -OH (for polymer) and –Si-OH (for silica). These end groups can ionize to produce a surface charge. When the colloids are suspended in a solvent, the surface charges attract free ions of the opposite charges from the solvent and form the outer diffuse layer. As a result, there is an electrical double layer surrounding the colloidal particles. Further, chemical compounds (salts) can be added to the suspension to control amount free ions in solution and hence the thickness of the electrical double layer.

The forces associated with the colloidal stability are due to the attractive van de Waals force and the repulsive electrostatic force on the surface. A stable colloidal suspension is the result of the higher repulsive force that prevents the particles from aggregation at a significant rate. In the case of high salt concentration, there will be more ionized free charged from the solvent adhering onto the particles' surfaces. Consequently the repulsive force decrease due to more screening effect. The higher attractive force will pull colloids towards each other and adhere strongly together

In general, colloidal particles are less affected by gravity and they are subjected to Brownian motion in suspension. Above a certain colloidal size, gravity becomes more important than Brownian motion. The lower bound of the colloidal size is at which the particles approach molecular dimensions.

Well-established procedures such as gravitation sedimentation or vertical deposition offer methods to self-assembled colloidal particles into opaline crystals as shown in figure 7(b). Although the phase diagram of colloidal suspensions is not fully understood, colloidal particles can be close-packed into a well-defined FCC structure. Particles' sizes on the order of the wavelength of visible light result in 3D crystalline structure with optical properties.

3.2 Self-assembly for Micro-fabrication

The rapid pace in microelectronic device scaling has called for a revolutionary shift from the present microfabrication techniques. The current research in self-assembly for nanotechnology shows it has the capability to address the challenges of ever-decreasing

dimension[41]. Whitesides Research Group[42] identified five key elements in order to make the nanotechnology viable. To meet the challenges in nano-scale manufacturing, there is a need for better process control in the nano-scale, be able to assemble system from nano-components, parallel manufacturing, three-dimension manufacturing and be cost effective. Self-assembly offers a number of advantages:

1) Self-assembly performs parallel fabrication processes.

2) Self-assembly builds structure with sub-nanometer precision.

3) Self-assembly generates 3D nano-scale structures.

4) Self-assembly allows process control through external forces.

Current c hallenge f or p erfecting s elf-assembly t echnique i ncludes t he c ontrolling the finite number of defects in the assembled structure. In addition, more research works a have to be carried out to improve on the efficient self-assembly manufacturing on a large scale and on the cost effectiveness.

Analogous to the spontaneous arrangement of material in nature, self-assembly in material generates a highly order three-dimensional structure that could have useful novel properties. For example, laboratory research showed the development of self-assembled photonic crystals with low defect densities[43]. In additional, three dimensional photonic crystals using colloidal self-assembly are presented in literatures[44,45]. In other research, molecular nano-scale structures with specific dimension and chemical properties were developed using self-assembly technique[46]. In summary, the self-assembly techniques provide new materials research and development in material science, microelectronics, photonic and data-storage[47] application.

3.3 Vertical Deposition Colloidal Crystallization

Vertical deposition colloidal self-assembly is a simple method for the fabrication of highly ordered porous structures[48] from a colloidal suspension. Figure 9 shows the schematic of vertical deposition. Though the mechanism is not well understood, it is commonly described as the assembly of colloidal particle by the capillary force of the meniscus as the solvent evaporates.
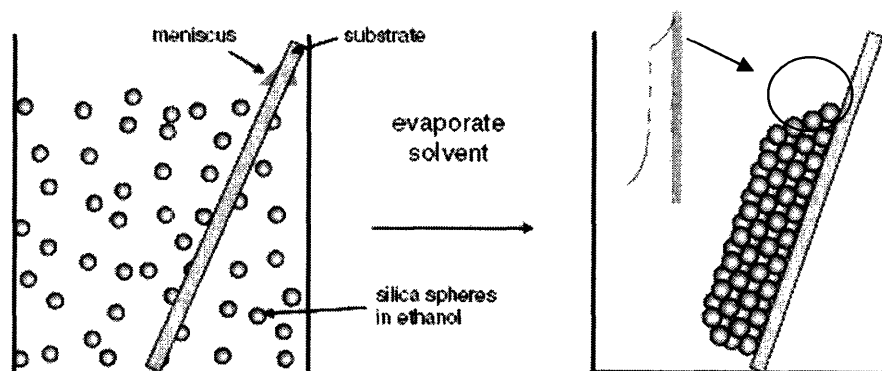
Figure 9. Organization of ordered colloidal crystal through vertical deposition with relatively uniform thickness.

Good quality thin colloidal crystal film can be achieved by using vertical deposition[49,50,51]. The capillary force created by the receding meniscus which arranges the particles in to a close-packed FCC structure, which correspond to the lowest energy state[52,53]. After deposition, it was found that the particles adhered well to each other and to the substrate. Infiltration of semiconductor material into this crystal was possible to create a photonic crystal. In the initial research phase, only particles of size 400nm or smaller was found to be possible through the vertical deposition. Larger size particles were found to be sediment quickly and did not deposit on the substrate. Later, a temperature gradient is implemented across the vial in order to achieve a stronger convective flow in the suspension. Size as large as 800nm is possible for vertical deposition. The larger colloidal particles enable the implementation of photonic crystal for the important 1.3μm or 1.55μm photonic applications[30, 43].
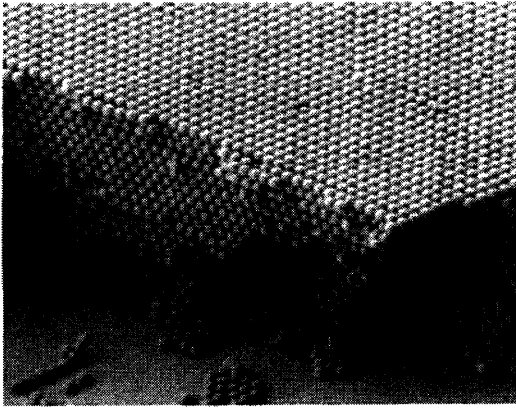
Figure 10. SEM image of the cross-section of an opal made from 1000nm silica particles [54].

Vertical deposition is an improved process over the sedimentation and the convective process. Figure 11 illustrates the sedimentation process where the stable colloidal suspension is left to stand. Over time, through Brownian motion and gravitational force, the particles and settle aggregate on the substrate in a fairly ordered structure. In addition, the solvent thickness and rate of evaporation play influence the ordering of the colloidal crystal[55]. At the edge of suspension bead on a hydrophobic surface, a solvent contact line formed which encourage convective flow (refer to figure 11(c)). The contact line is pinned during the evaporation. The drop of solvent ensures that liquid evaporating from the edge is replenished by liquid from the interior[56]. The resulting outward flow can carry dispersed material to the edge, resulting in a convection flow.
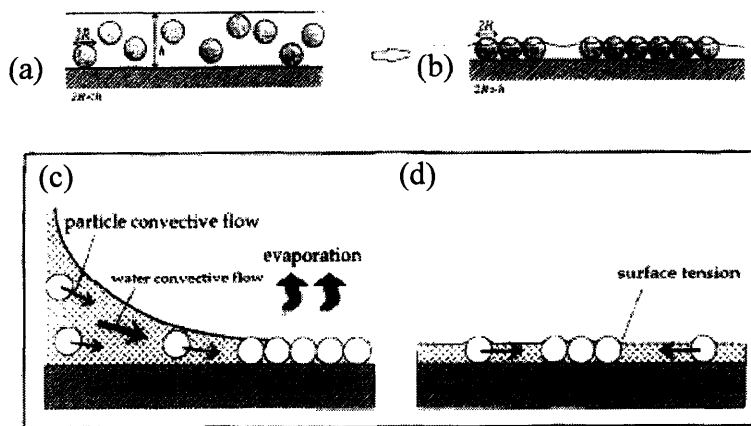
Figure 11. (a) Colloidal particles under the influence of Brownian motion and gravity. (b) Colloids assemble when their thickness is comparable to the thickness of the thin liquid film. (c) Evaporation of solvent creates the convective flow of solvent and causes the particles to move towards the boundary. (d) Surface tension of solvent create the lateral capillary force to pull particles together.

26

3.4 Electric field-directed Colloidal Crystallization

In the previous section, nucleation of colloidal particles from an aqueous suspension was analyzed. To form a well-ordered crystalline structure, various deposition techniques were carried out so that these colloidal particles could self-assembled in a longer-range order.

Here, utilizing electric field in assistance to the self-assembling of colloids is discussed. It is well known that charged particles under the influence of a static or dynamic electric field experience electrophoretic forces[57]. Application of electric field to produce crystalline colloidal structure was first report by Richetti et al[58]. The electric field attracts charged colloidal particles and causes them to move towards the electrodes or be aligned along the electric field. Since the colloids are in suspension, an electrohydrodynamic flow mechanism describes the behavior of colloidal particles assembling into 2D or 3D structures[59]. Electric field-assisted self-assembly allows micro-patterned colloidal crystals through lithographically patterned electrodes[60].

The electrophoretic assembly of colloidal crystal offers an improvement over the traditional colloidal crystal self-assembly through its quicker crystallization rate and higher controllability of the crystallization process. The usual sedimentation or convective self-assembly technique is largely a lengthy process, which depends on the rate of evaporation of the solvent. On the other hand, the speedier electrophoretic assembly process offers more control and is dependent on parameters such as strength of electric field, current density, field cycling[61], colloid surface charges and the ionicity of the electrolyte[62].

A well-cited paper on electrophoretic assembly of colloidal crystal[59] in 1996 envisioned and demonstrated the possibility to assemble two- or three-dimensional colloidal crystal on electrodes precisely. Figure 12(a) shows the in-situ experimental setup with the transparent indium tin oxide (ITO) and metal piece as the anode and cathode respectively, the middle cavity was filled with dilute colloidal dispersion. Under the influence of electric field, the electrophoretical behavior of the colloidal particles was observed using a microscope. Figure 12 depicts the direct current (dc) and the alternating current (ac) methods of electrophoretic assembly of negatively-charged particles (PS microspheres).

27
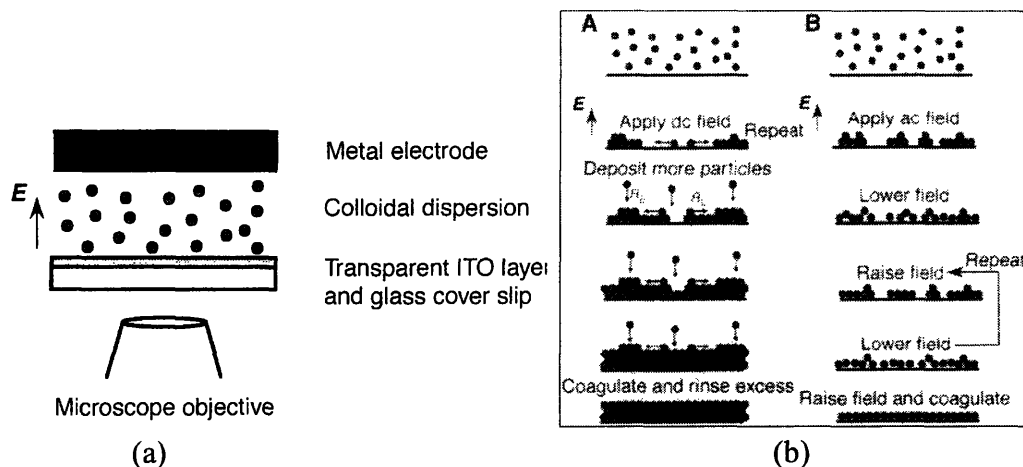
Figure 12. Electophoretic deposition of colloidal particles. (a) Microscope monitoring on colloidal particles under electric field, anode is the ITO glass and cathode is the metal; (b) Schemes of assembling colloidal particles into ordered layers using DC and AC electric field. Lateral force (induced by higher current density or Brownian motion) causes highly ordered layers[59].

The observations were (values quoted are experimental):

1. Under low dc or ac electric field (10V/cm), the colloidal particles formed island-like clusters on the anodes;

2. Above a certain ac frequency (1MHz), the clusters had little or no adhesion to the anodes due to no net electrostatic force pulling them towards the electrodes (1khz was used);

3. Increasing applied electric field (40V/cm) and higher current density (~100 μA cm^{-2}), the colloidal particles moved across the surface of the electrodes, this lateral movement result in the formation of mono- or multi-layers;

4. Cycling a low and high electric field also result in layer assembly: during high field the colloidal particles were attracted towards the electrode, and during low field Brownian agitation caused the colloidal particles to move randomly and form layer arrangement.

The paper[59] outlined the general phenomenon and observation of electrophoretic deposition of the colloidal crystal. In essence, the similarly charged colloidal particles overcame electrostatic repulsion when they approaching each other during the electrophoretic process. The electric field strength created sufficient attractive interaction

28

for the colloidal particles to come together. One important by-process of the electrophoresis is the electrolysis of water[60]. On a separate note, current density was kept low ($<$ 1mA cm^{-2}), which allowed H_2 and O_2 products to be transported away from the electrode surface[63] and hence bubble formation was not observed. In the ensuing work[64], the group reported selective positioning of negatively charged PS microspheres on ITO anode when illuminated with UV-light. Colloidal particles, attracted to the electrodes and randomly positioned, could be swept from the darkened area into UV-lighted region. This gave one more control parameter because the intensity and the location of the UV-illumination moderate the colloidal assembly process. Figure 13 shows the UV scheme of selective assembly of colloidal particles.

Using electrophoretic deposition, 2D micropattern of colloidal assembled layers can be preferentially deposited onto lithographically patterned electrodes[65]. Figure 13(a) shows the scheme of deposition of the PS particles onto the gold patterned electrodes. This method is based on the higher current density in the vicinity of the gold electrodes, which attracts the PS particles. The figure also illustrates the aggregation of PS particle in the non-patterned region due to convective flow and non-zero electric field (ITO conductor). In figure 13(b), the assembled 2D layer of PS has a shorter range order compared to the earlier experiment [59] and this needs to be improved on in order to present a useful photonic material.
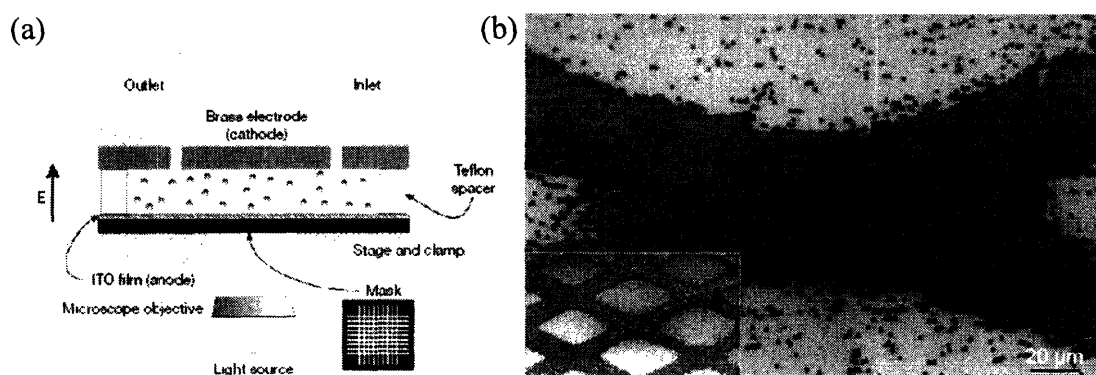
Figure 13. Colloidal particles deposition on anode electrophoretically and assembly under UV-illumination selectively. (a) The grid pattern defined the areas when the ITO glass (anode) is lit with UV-light. (b) Scanning electron microscope (SEM) image of the assembled colloidal particles under UV-illumination.

3.5 Template-directed Colloidal Crystallization

Pattern transfer using photolithography is the important process in microelectronic fabrication. Borrowing the same idea in colloidal self-assembly, pattern or template is created on the substrate where the colloidal crystallization is directed. In order to produce functionalized photonic crystal such as filters, switches, waveguides or lasers, the structures of the photonic crystals has to be properly designed. The template could be a layer of photoresist and patterns are created through photolithography and striping. The template provides a mean to control the lattice structure, orientation and size of the resulting colloidal crystal[66]. Further, templates can create the defect patterns on existing colloidal crystal to order to achieve waveguiding or resonant cavity structures. Aiding colloidal particles in depositing into the templated surface, external factor such as topographical surface confinement[67], electrostatic force[68] or wettability differences on surface[69] can play a critical role.
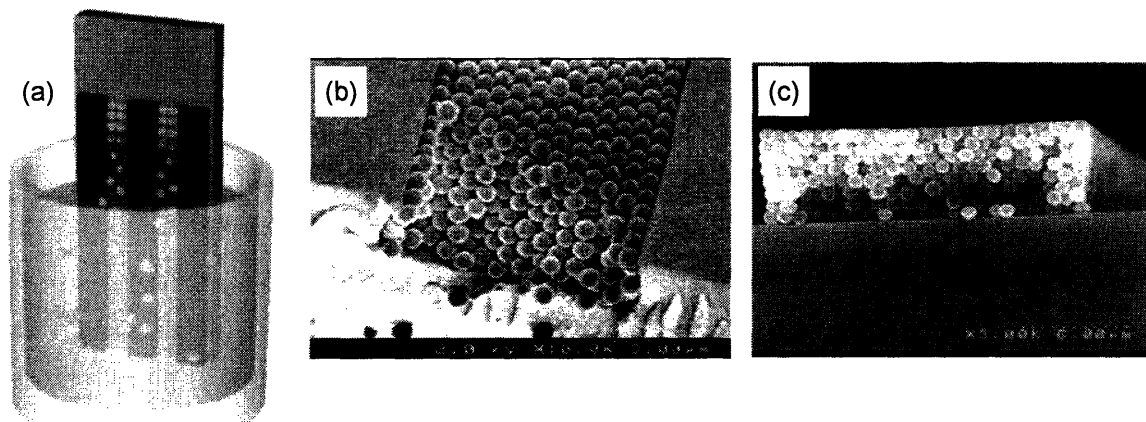
Figure 14. (a) Template-directed colloidal crystallization with vertical deposition and evaporation processes. SEM images of the micro-channel (b) before and (c) after stripping the template (PDMS).

Figure 14 shows an example of template-directed colloidal crystallization through topographical surface confinement . Yang et al[67] demonstrated this evaporated induced self-assembly method to create patterned 2-dimensional micro-channel with uniform

30

thickness. This is useful to create planarized micro-photonic chip where waveguides structure can be created on a substrate. Figure 14 depicts the SEM images of the micro-channel before and after stripping the poly-dimethylsiloxane (PDMS) pattern. The template can also define patterned electrodes so that electric field deposition can aid in the colloidal crystallization. According to Kumacheva et al[68], photo-resist is spin-coated on an ITO glass substrate. Pattern is defined lithographically where the ITO is exposed to be the anode. Figure 15(a) illustrated the schematic of the experiment where electric field is used to attract negatively charged poly-methylmethacetlate (PMMA) colloidal spheres towards the anode. Self-assembly of micro-spheres on a patterned electrodes under the influence of an applied electric field was demonstrated. The dimension of patterned ITO anode was carried designed so as to allow close-packed colloidal array to form (figure 15(b)). For cases like chemically patterned surfaces, the wettability differences on surface can result in patterns of colloidal array assembly[69]. Selective surfaces of a PDMS surface can be treated with plasma oxidation and result in hydrophilic / hydrophobic pattern. A colloidal suspension drop on these surfaces results in the spilt of the drop in the evaporation. The colloids are drawn from the hydrophobic surfaces to the hydrophilic surfaces via the wetting / dewetting process. Through a convective process in the hydrophilic surface, the colloidal particles are drawn to the drying front where they are close-packed to form an ordered colloidal assembly.
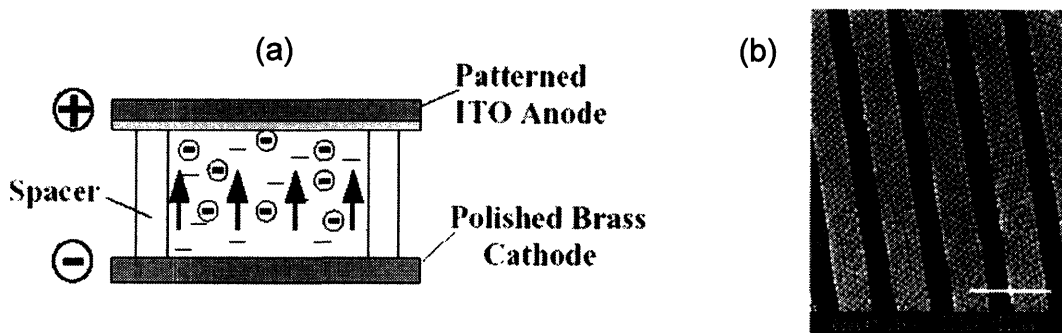
Figure 15. (a) Experiment setup for the self-assembly of negatively charged PMMA micro-spheres under the influence of electric field from the patterned ITO anode. (b) SEM image of the colloidal array electrodeposited on the patterned ITO anode.

31

To insert line defects in colloidal crystals, a recent progress[70] in advanced colloidal self-assembly using photolithography is shown in figure 16. Using a 2-stage colloidal self-assembly, silica infiltration and a templated definition stages, a hollow air-core line defect can be embedded into the inverse opal structure. This method can be pursued to achieve a waveguide for photonic integrated circuit application.
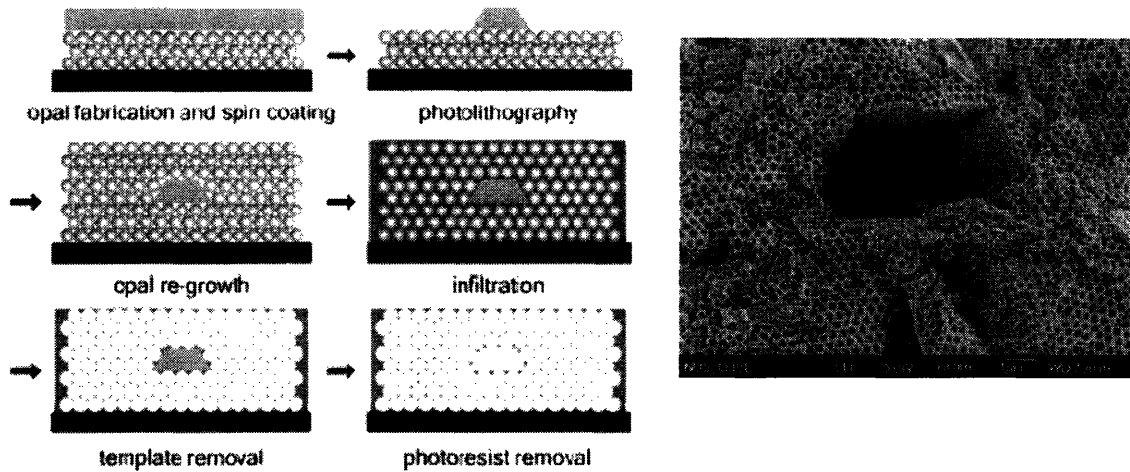
Figure 16. (a) Schematic of incorporating an air-core line defect in the colloidal crystal. (b) SEM image of the cross section.

3.6 Ionic Colloidal Crystallization

Ionic colloidal crystal (ICC)[71] is a new class of material that could manifested as a variety of structures through the mixture of multi-component building blocks. Unlike the one-component suspensions which can self-assemble into FCC structure under suitable condition, multi-component system can exhibit a rich variety of crystalline structures[72,73]. Thus, ICC has potentially broad range of novel and tunable properties and is a promising material for photonic, catalysis and filtration applications. In photonic application, the ICC offers an excellent way to achieve structure engineering, for example, to produce a diamond structure (complete photonic bandgap) or zinc blende structure[74] (complete photonic bandgap at even lower refractive index constract). Potentially, ICC enables the implementation of a novel photonic bandgap material with less restriction on the choice of raw materials.

Analogous to those in atomic ionic compounds, ICC is made up of positively and negatively charged colloidal particles[75]. These two-component colloidal crystals are stabilized by long-range attractive electrostatic interactions by specially tailoring the conditions where it is energetically and kinetic favorable to aggregate into ICC. Maskaly et al[74] constructed a model of stability of ICC by evaluating the Madelung summation to give the electrostatic energy of ICC. Particle interaction forces such as van der Waals and gravitational forces are not considered in the computation. The result can be summarized in the phase stability diagram as shown in figure 17. The phase stability diagram described the type of structures ICC might adopt as function of the ratio of the positive/negative particles' charges and the spatial extent of the electrostatic interaction. The favorable kinetic condition to crystallize into ICC structure (over maintaining in dispersed form) is that the experimental temperature must be above the glass transition point. This is based on the diffusion of particles to their ordered state is thermally activated. Further, there is a critical temperature above which the particles are attracted to oppositely charge particles. This ICC critical temperature can be lowered by reducing the interaction among the particles through (i) reducing the surface charge, (ii) increasing particle size.

33
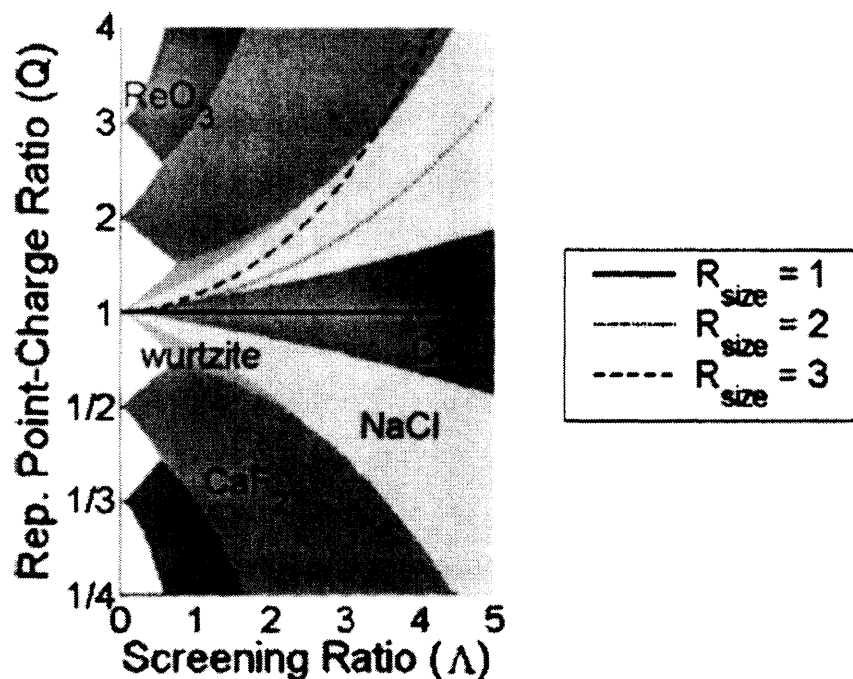
Figure 17. Phase stability diagram of ICC. The six structures are ruthenium oxide, fluorite, wurtzite, rocksalt and cesium chloride. The phase identified the most stable of the six structures where the largest Madelung sum is taken. Vertical axis is the representative point-charge ratio (continuum charge ratio due to varying charge in a particle) and the horizontal axis screening distance relative to the particle size. The size ratio (Rsize) of binary colloidal particle is taken to be 1 (default), 2 and 3.

In another independent study on oppositely charged colloidal particles, Bartlett et al[76] varied the surface charge of particles when keeping the spheres size constant. They demonstrated the ICC switched between FCC, cesium chloride, and sodium chloride structure, figure 18. They suggested that transformation among the different structures is related to the competition between the entropic and Coulombic forces. Agree with this hypothesis, Leunissen et al[77] demonstrated that through experiment and simulation the tuning o f e lectrostatic c harges o f o ppositely charged p articles r esult i n t he f ormation o f ICC. Hynninen et. al. did another independent studies on the ground-state phase diagram of ICC[78] based on Madelung energy computation using screened Coulomb potential. Figure 19 illustrated the ground-state phase diagram of ICC with more variety of structures considered. Through experiment, three of the phases (LS_8^{hcp}, LS_8^{fcc} and $A_6C_{60}^{bcc}$) are validated under the observation of confocal microscopy, see figure 20. Hence, the theoretical computation provides a useful tool to predict the resultant ICC structures.
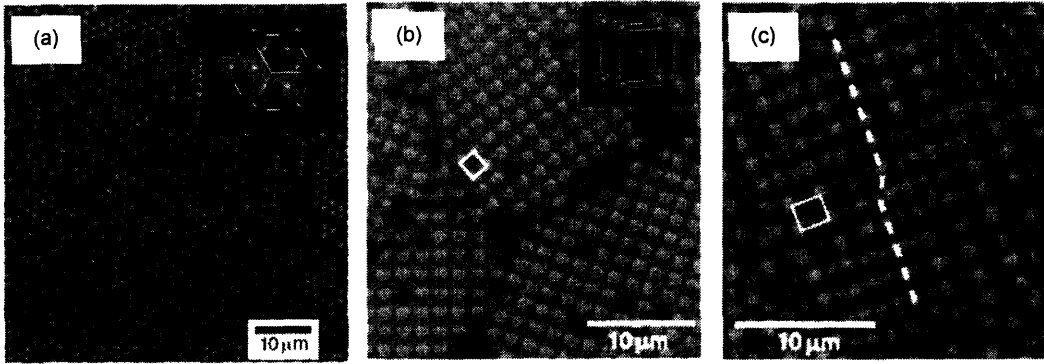
Figure 18. Confocal images of FCC, cesium chloride, and sodium chloride structure.
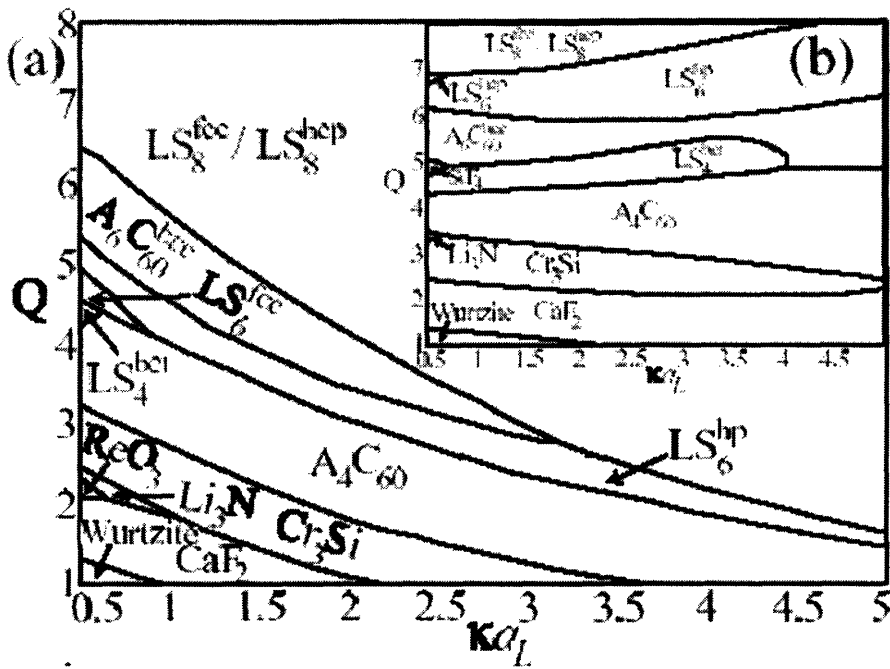
Figure 19. The ground-state phase diagram of ICC with fixed composition of small and large colloidal particles. A plot of charge ratio Q against the reduced screening constant κaL. Size ratio of small to large colloidal particles is 0.31. (a) The structure coexisting with an infinitely number of pure small colloids, (b) The structure coexisting with an infinitely number of pure large colloids.
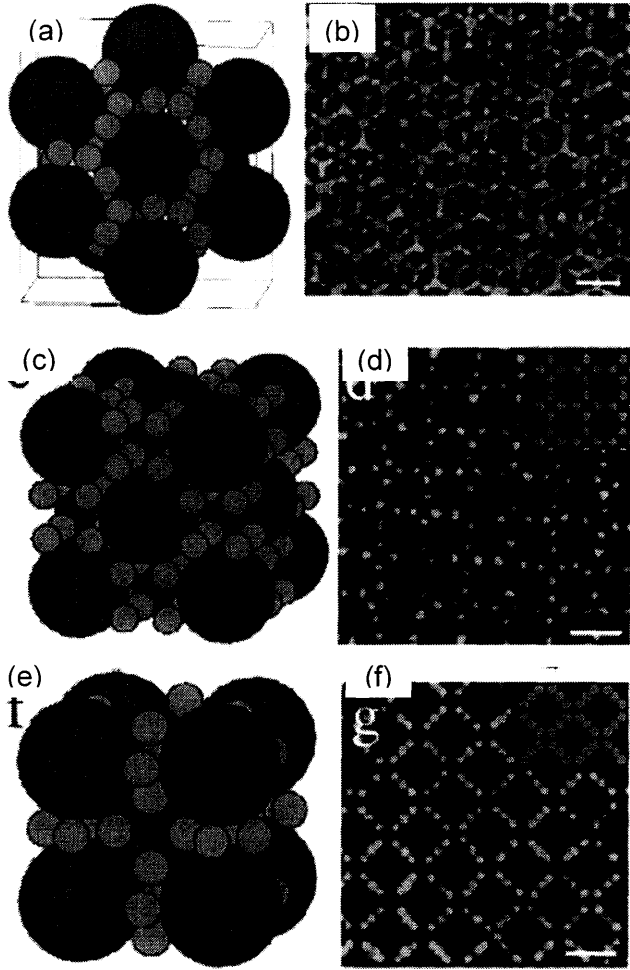
Figure 20. Confocal microscopy images of ICC binary structures. (a) and (b) are the unit cell and the confocal image of LS_8^{hcp} respectively, (c) and (d) LS_8^{fcc}, (e) and (f) $A_6C_{60}^{bcc}$.

Self-assembly of ICC offers a revolutionary way of engineering the structures that is of attractive properties. Such method is ideal for achieving a diamond lattice photonic crystal that has a complete bandgap to control the flow of light. Making use of computation analysis to study ICC stability phase diagram, a specific structure can be design for diamond unit cell, figure 21. Using different materials for the large and small colloidal particles, selective etching can be carried out after the ICC has been formed. The large colloidal spheres can be the main building blocks for the diamond structure while the

36

small spheres can be the scald-folding for the large spheres. Then, the small spheres are etched away, resulting in the diamond structure[79].
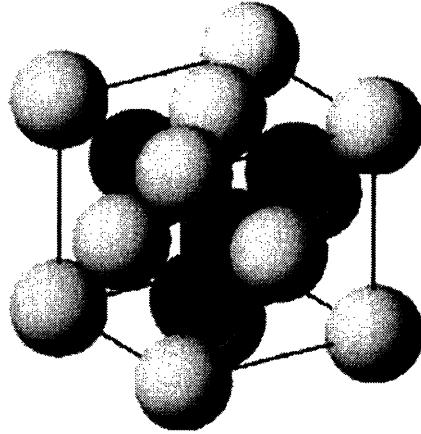
Figure 21. The unit cell of a diamond structure.

4.0 Assessment of Colloidal Self-assembly for Photonic Crystals

The first successful demonstration of inhibiting the propagation of electromagnetic wave by E. Yablonovitch using an ordered dielectric structure has since generated significant interest on the research of photonic crystal. The early photonic crystals were fabricated using well-developed microelectronics processing technique. Later, reports by A. van Blaaderen and S. John on the possibility of using self-organized dielectric spheres to create photonic crystal fueled the research and invited fresh ideas from the colloid science fraternity. Development in colloid science has been a major boost for the material research into photonic application. Self-assembled colloidal crystals provide building blocks or templates to fabricate photonic crystals. Starting from year 1995, there is a steady grow in the research papers on colloidal photonic crystal, as shown in Figure 22. Experimental results on optical measurement were reported in the late 90s and optical property had been quickly improved ever since. Advances and maturity in the processing result in longer range order and the reduction of defects in colloidal crystal. A reflectivity 100% at centre of photonic bandgap can be demonstrated.
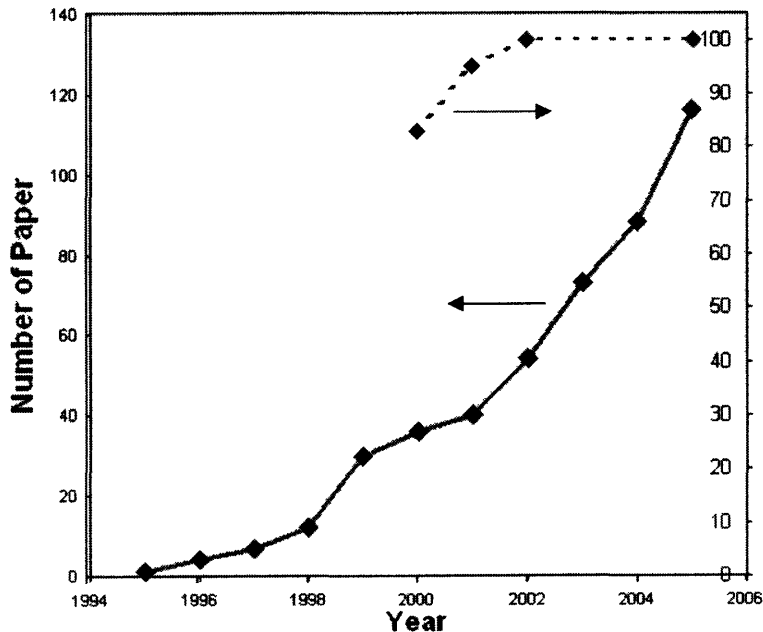
Figure 22. A plot of the number of papers published yearly on colloidal photonic crystal between 1995 and 2005 (solid line). Source: ISI Web of Science. Reflectivity measurements of photonic crystal reported between 2000 and 2005 (dashed line).

4.1 Category and Processing Techniques

Colloidal particles or microspheres self-assembled into colloidal crystal, also known as synthetic opal. Since a colloidal crystal has ordered structure, it satisfies Bragg's Law when a beam of light is impinged on the crystal and diffracted. Hence, the colloidal crystal is described as a photonic crystal loosely. However in stricter sense, a photonic crystal should have a well-defined band diagram complete with photonic bandgap. Accordingly, this colloidal crystal becomes a template for semiconductor material infiltration as described before. After the removals of template using calcination or HF etch, the resulting structure is commonly known as the colloidal photonic crystal or the inverse opal. In short, the colloidal photonic crystal is a three-dimensional bulk crystal that has undergone crystallization processes by self-assembling colloidal particles. This bulk photonic crystal has applications in electromagnetic wave filter and reflector. Photonic application of bulk photonic crystals is demonstrated in the implementation of optical notch filter[80]. An inverse opal exhibit a photonic bandgap that prohibit the propagation of electromagnetic wave at a designated wavelength. Thus, filtering of a signal is best exemplified by the photonic bandgap.

1. Crystallization	2. Device Functionalization
(a) Sedimentation	(a) Lithography / etching
(b) Vertical Deposition	(b) Chemical Vapor Deposition
(c)Template-directed deposition	(c) Electrochemical plating
(d) Electro-deposition	(d) Langmuir Blodgett
(e) Ionic colloidal crystallization	(e) Spin coat
(f) Material infiltration	(e) Electron-beam lithography
	(f) Multi-photon polymerization

Figure 23. Category of Colloidal Photonic Crystals and their processing.

On the other hand, the bulk photonic crystal can be functionalized as optical switches, waveguides or laser. Materials of unique property can be infiltrated, deposited via CVD in an inverse opal, which is a highly porous structure. For example, optical switches[81] are made out of inverse opals in an aqueous medium, whose refractive index is stable against temperature change. The inverse opal is immersed in the hydrogels solution, figure 24. Under low light intensity the hydrogel and the colloidal crystal's refractive index are matched and do not diffract light (Bragg's diffraction). However, under high intensity the inverse opal absorb light and get heated within nanoseconds, resulting in a lower refractive index than hydrogel medium. Consequently, there is a periodic refractive index modulation in the crystal and light is diffracted. Consequently, this results in optical switching which responds to the intensity of light within nanosecond.
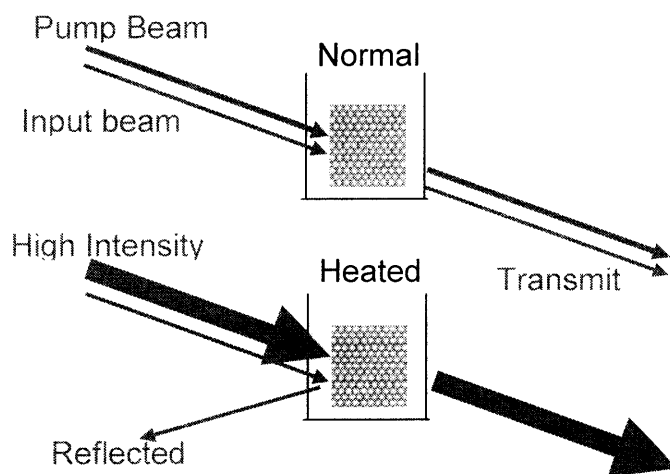
Figure 24. Optical switch using colloidal photonic crystal in hydrogel aqueous solution. Top: Input beam transmit through when the pump beam has a low intensity. Bottom: Input beam reflected when the high intensity pump beam changes the refractive index of the inverse opal.

A photonic band gap is useful to inhibit the propagation of electromagnetic waves however it is desirable to have a propagation mode in the gap for application in optics and optical computing[82,83]. Therefore it is necessary to introduce well-defined defects (localized modes) into the photonic colloidal crystals so that there is precise guiding of photons through the localized modes inside the photonic band gap. A point defect results in a cavity, line defect is like a waveguide and planar defect results in bandgap engineering. These defect modes can be tuned by adjusting defect volume and the dielectric constants of

the dopants[84]. However it is a great challenge to engineer extrinsic defects into colloidal photonic crystals via a bottom–up self-assembly approach[85]. A planar defect is introduced by sandwiching the dopants between colloidal crystal layers by Langmuir–Blodgett (LB)[86] or spin-coating[87] techniques. Figure 25 shows a SEM image of a planar defect[88] sandwiched between two inverse opal layers. The thickness of the planar defect has an influence on the resulting wavelength of localized mode within the photonic bandgap, exemplified by a dip in the reflectance spectrum (dashed line) in figure 25(b).
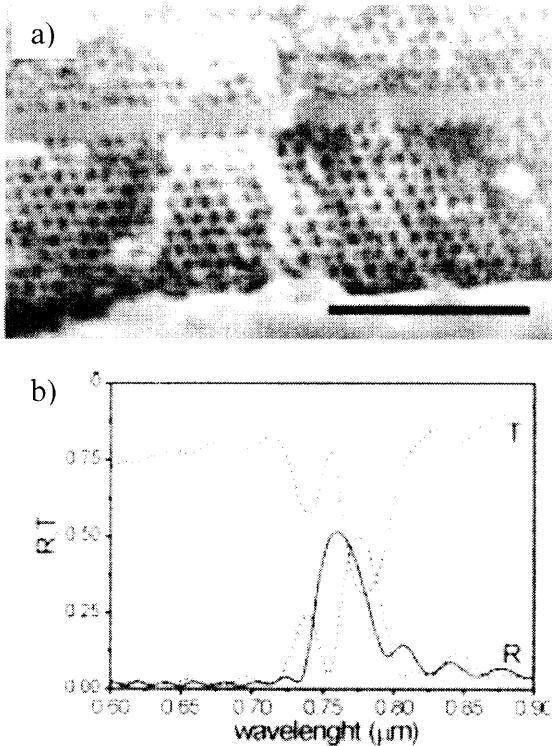
Figure 25. (a) Introducing a silica sandwich between two inverse opal layers. (b) Spectroscopy measurement: reflectance spectrum of the inverse opal without silica sandwich (solid line); reflectance and transmittance of the inverse opal with silica sandwich (dashed lines), a dip of reflectance (dashed line) around 0.75um wavelength indicates a propagation mode in the photonic bandgap.

Further, to functionalize a colloidal photonic crystal, photolithography / etching can be employed to create patterns on the crystal. For example, a line pattern is lithographically defined and etched away to create a line defect for a waveguide application. Other advanced method includes electron-beam lithography[89] and multi-photon polymerization techniques, figure 26. Often, there is a need to have another crystalline layer deposition over the line defect in order to realize a confined 3D waveguide structure.
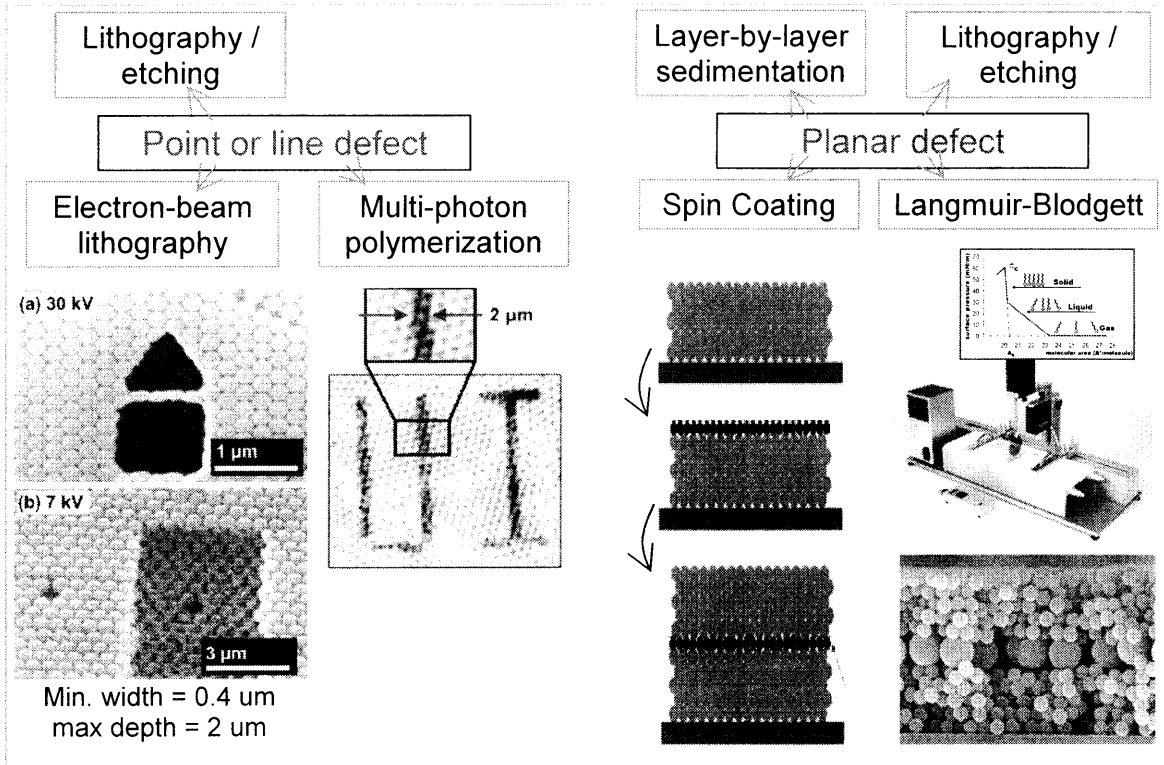
Figure 26. Some examples of photonic crystal devices functionalization processes to incorporate point, line or planar defect.

4.2 Progress in Optical Performance

The unique optical property of a colloidal photonic crystal is its ability to inhibit the propagation of electromagnetic wave at a particular wavelength. Here, the reflectivity of an inverse opal is studied as a measure of its optical performance and the photonic bandgap's usefulness. Figure 27 shows the band diagram of a silicon/air inverse opal arranged in a FCC structure. As mentioned in the chapter 2, the inverse opal exhibit a gap between the 8th and 9th bands if the refractive index contrast between the infiltrate dielectric material and air spheres is greater than 2.8[90,91]. Silicon has a refractive index of 3.5 approximately about optical wavelength range. Further, a pseudo gap between 2nd and 3rd bands forms when the dielectric/ air matrix has a FCC structure and is largely unaffected by the refractive index contrast.
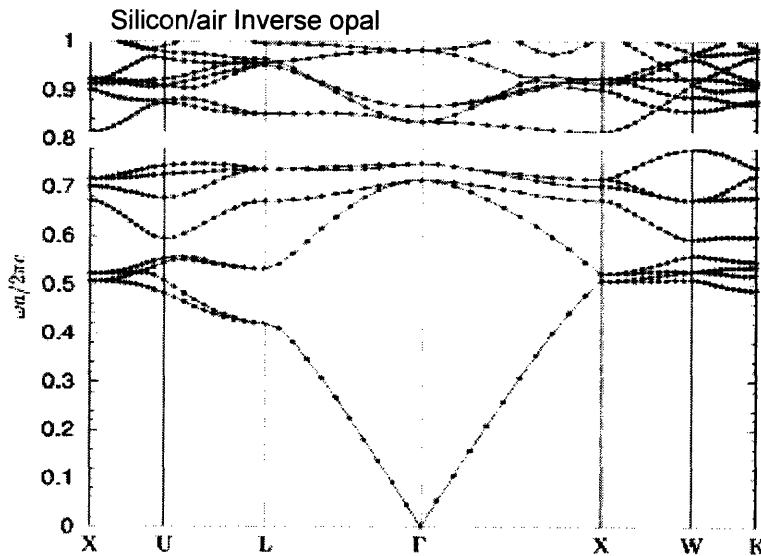
Figure 27. The photonic Band diagram of a silicon inverse opal. The top long strip corresponds to the complete gap between the 8th and 9th bands. The center wavelength of the complete gap is $a/0.79$, where a is the lattice period. The bottom strip is the pseudo gap between the 2nd and 3rd bands. The center wavelength of the pseudo gap is $a/0.48$.

The spectral position and the spectral width of the optical gap depend on the lattice period (a) and on the relative dielectric/air refractive index (n). The center wavelength of the complete and pseudo gap is approximately at $a/0.79$ and $a/0.48$ respectvely for silicon/air matrix system. By changing the colloidal microsphere size and hence the lattice period, the spectral position of the gap (wavelength) can be adjusted. In summary, the

43

refractive index contrast and the lattice period influence the wavelength of electromagnetic wave to be inhibited or reflected.

An optical reflectance spectroscopy experiment was done on a close-packed silicon inverse opal structure[92], figure 28. The reflectivity measurement was conducted in the three principal directions from wavelength 1.2µm through 6.6µm and the reflectance profiles resemble to that of the band diagram. Reflectivity was relatively high around the wavelength of the complete bandgap, especially at the center of the gap. A nearly 100% of reflectance was achieved in [111] and [100] direction, while only 55% reflectivity was measured in the [110] direction. Cracks or shorter range order might be the cause for the lower than expected reflectivity measured in the [110] direction. The reflectivity measured at the pseudo gap wavelength was close to 100% for [111] direction, which correspond to L *k*-space in figure 27.
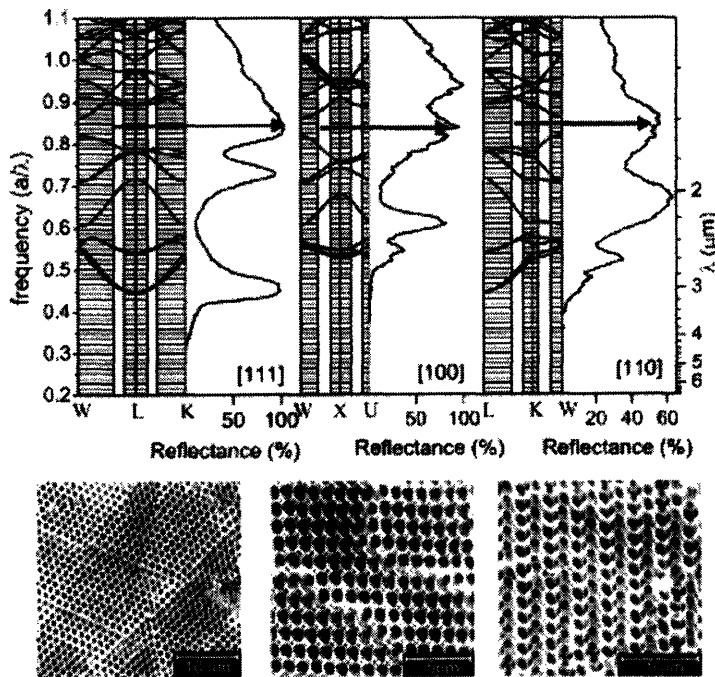
Figure 28. The measured reflectance spectra of a silicon inverse opal structure. The SEM images of the three principal surfaces, L [111], X [100] and K [110].

The optical performance of a silicon inverse opal can be compared to that of a woodpile structure, fabricated with microelectronic technique. Figure 29(a) shows the experiment result of a widely cited paper[21] and the reflectivity of the 7-layers silicon inverse opal was between 95% ± 5% in the photonic bandgap. On the other hand, Lin et al

44

reported a reflectivity of 90% ± 5% in the photonic bandgap for a 5-layer woodpile structure[93]. In this comparison, the optical performance of colloidal photonic crystal is slightly better and it shows that colloidal crystal has come long way to match the quality of the traditional photonic crystal made by the microelectronic processing. Over the year, the improving controls in the defect, crack formation and the reduction disorder in the colloidal crystal have driven the successful of the colloidal photonic crystal. It may be argued that the inverse opal has more layers than the woodpile structure, thus giving superior performance. However, fabricating an inverse opal structure is much more simple and economical process than the woodpile structure.
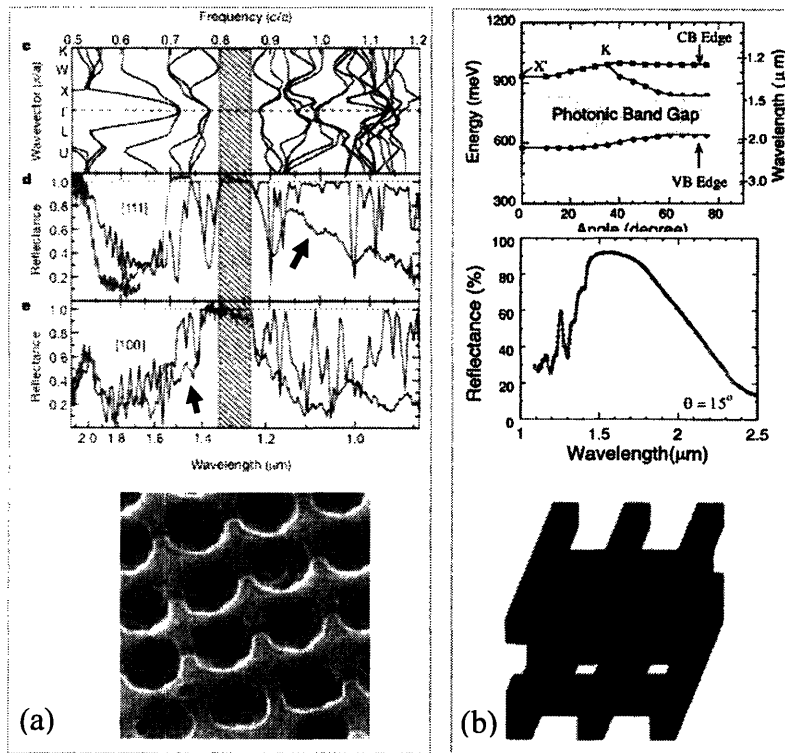
Figure 29. The reflectivity measurement. (a) 7-layer silicon inverse opal. Arrow pointing the graph (red line) of the reflectance. Reflectivity is 95% ± 5% in the gap. (b) 5-layer woodpile structure. Reflectivity is 90% ± 5% in the gap.

In addition, figure 30 shows the spectral position (a/λ) of theoretical peak reflectivity versus the experimental peak reflectivity. Ideally, the theory used to calculate the photonic bandgap or optical performance assumed that the crystal is infinite in size. Practically, the thickness or the number of lattice layers is finite and a balance must be resolved. In another experiment, Lopez et al[94] investigate the finite size effect of an inverse

opal structure. Figure 30 shows a plot of the center bandgap (peak reflectance) versus the number of layer of the inverse opal (at pseudo gap, frequency = 0.605). It was found that an approximately 40 layers of colloidal particles are needed before it would closely follow the theoretical prediction of the center bandgap spectral position.
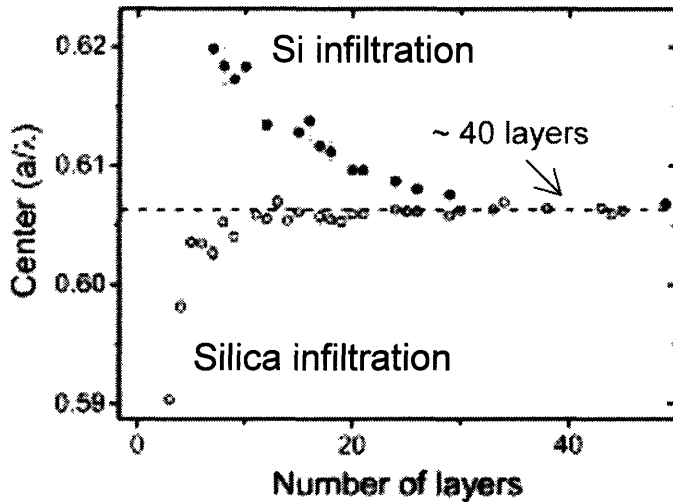
Figure 30. The plot of peak reflectance spectra as a function of number of layers in an inverse opal. The horizontal dashed line is the theoretical data for an infinite size structure. The experimental data are filled circles (silicon) and open circles (silica).

4.3 Disorder Effect on Optical Properties

The effect of intrinsic disorder introduced during the growth of the colloidal crystal is discussed next and it has an impact on the optical properties of the colloidal photonic crystal. Structural disorders, voids or cracks are the light scattering centers. This causes coherent beam of incident light to be scattered and results in diffused light[95].

In particular, the degree of polydispersity of the colloidal particles has an impact on the optical properties. The colloidal microspheres defined the periodicity of a photonic crystal, and when the sizes of the microspheres are non-uniform, the ordered structure is disrupted. It was found that polydispersity of >3% the colloidal crystal loses its ordered structure and becomes randomly packed[96]. In a computer simulation study, the onset of the disappearance of photonic bandgap is when the variation in the radii of the microspheres is more than 2% of the lattice constant[97]. Photonic bandgap is fragile due to the non-uniformity in crystals.

The inverse opal was found to be fairly robust to stacking disorder[98]. Even in the event of totally random stacking sequence, the simulated transmission spectrum is able to

compute the presence of photonic bandgap. The total random stacking disorder manifested as p ronounced d ips w ithin t he f requencies o f t he c omplete g ap (8th a nd 9th b ands). T he pseudo gap is found to be untouched by stacking randomness due to the weaker effective perturbation in lower frequencies.

Substitutional point defect or a missing colloidal particle in the crystalline structure introduces a l ocalized m ode i n t he p hotonic b andgap. This c reates a m icrocavity w here light is trapped. This intrinsic defect is an ideal functional block for a photonic integrated circuit chip, especially for light amplification in laser or signal coupling to another channel in a resonator coupler. For bulk photonic crystal application, the point defect manifested as a slight dip in the reflectance spectral[99].

Cracks are commonly observed in a colloidal crystal film. Typically, the crack size ranges from a fraction to a few microspheres' diameter. The cause of crack formation during colloidal self-assembly is the solvent drying process where the close packed colloidal array shrinks further and gives rise to cracks[100]. For large area colloidal photonic crystal application, cracks do not affect the optical properties to a large extent[101]. This is especially so for cracks density of <1% (count visually across a surface in a straight line, number of crack per micropsheres) which is common in the self-assembly process. However, for photonic integrated circuit application, crack is a great concern where attenuation and cross-talk would impair signal integrity.

In summary the effect of the disorder on colloidal photonic crystal is listed as following:

1. Radii fluctuation > 2% of lattice constant

   Photonic bandgap ceases to exist in a randomize simulation.

2. Poly-dispersity > 3%.

   Ordered structure goes random and no longer in crystalline structure.

3. Stacking disorder

   Photonic bandgap stays fairly robust even in total random stacking disorder.

4. Point defect

   Localized mode introduces in gap and hence light is trapped.

5. Cracks

   Light scatters and bad for signal integrity sensitive application.

4.4 Optical Properties Improvement Techniques

The ability to control of their photonic crystal optical properties accurately is crucial to realize useful photonic devices. In general, the control of colloidal sizes and dielectric constants enable the tailoring of frequency of operation in a colloidal photonic crystal. Besides, intrinsic defects affect the photonic crystal's optical properties in varying degree as described previously. Studies have shown that crystallization under confined volume or patterned substrate can produce large area colloidal crystal film free of defect and stacking disorder.

In application where only small area colloidal crystal film is required, micro-channel pattern[102] on substrate can be the excellent template-aided self-assembly tool. Volume confinement of colloidal microspheres in microchannels has shown to give high quality crystalline colloidal crystal over hundreds of length with a very low concentration of intrinsic defects. Figure 31 shows the SEM images of the top view of the microchannels, pillars templates and the corresponding ordered colloidal crystal. Further, crystal size, shape, and orientation can be controlled precisely using template. The lithography system need not be high resolution and costly to create patterns for the templated self-assembly.
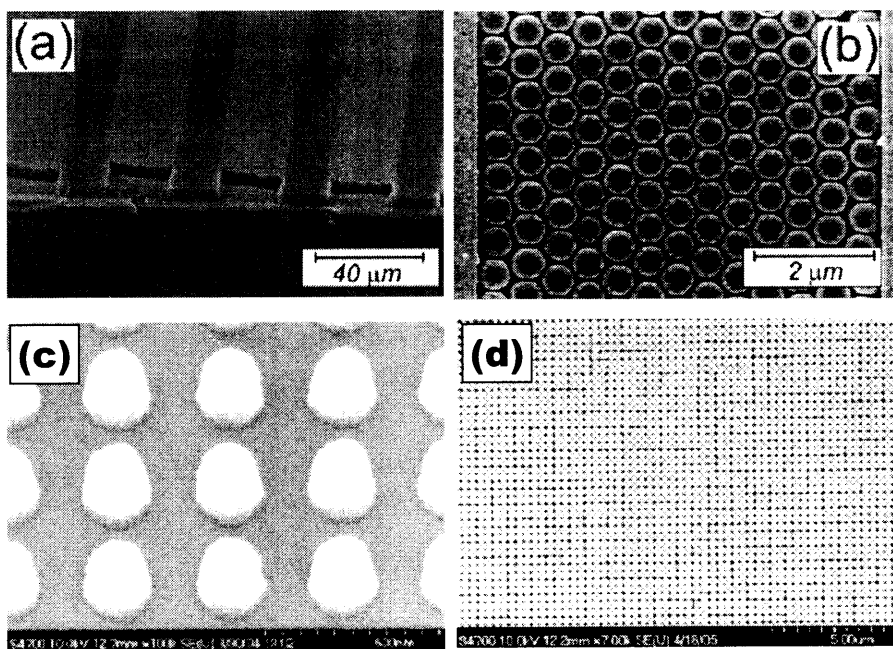
Figure 31 SEM images of templated self-assembly colloidal crystals. (a) Array of micro-channels, (b) top view of the crystalline structure inside a micro-channel. (c) Tilted view of the pillar-like template at 30°, (d) Crystal growth on pillar-like template.
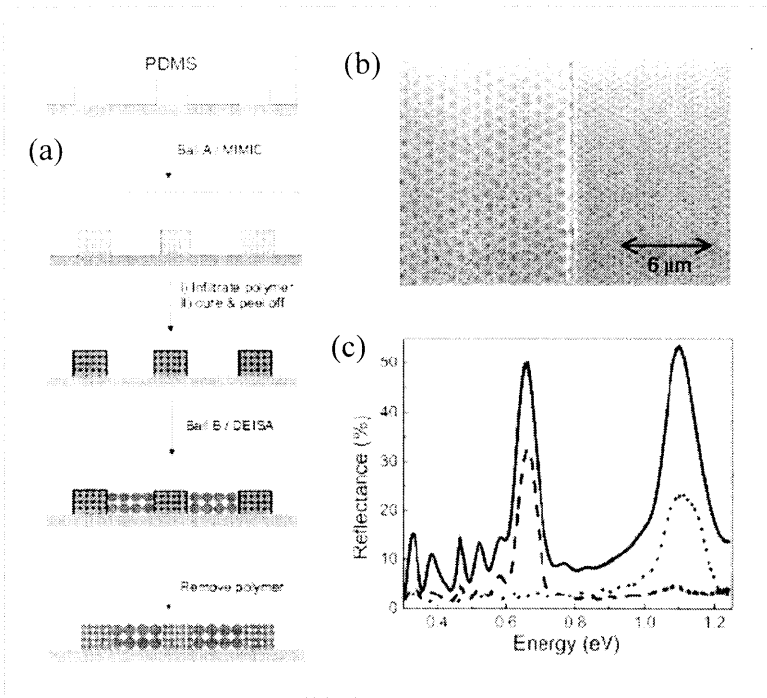
Figure 32. Heterostructure colloidal crystal (a) Schematic illustrating the fabrication of the heterostructure film on substrate. (bc) Top SEM view of the heterjunction. (c) Reflectance spectra of individual colloidal arrays (dashed and dotted) and the combined heterostructure (solid).

A heterostructure colloidal crystal can help to improve the reflectance spectra of individual crystal array[67]. The heterostructure colloidal crystal is made up of alternative array of different size colloidal particles. Figure 32 illustrates the procedures of fabricating alternating rows of colloidal crystal of different lattice period using soft lithograpghy. Figure 32(c) shows the experimental result of the reflectivity of individual arrays of different size microspheres and the combined heterostructure. It can be concluded that the optical properties improved for heterostructure (higher reflectivity) due to the result of adding up the optical properties of individual colloidal crystals.

4.5 Case Studies

This section discusses on the future development of colloidal crystal applications, their present shortcomings / advantages and how they can be improved.

4.5.1 Diamond Structure Colloidal Crystals

A self-assembled colloidal crystal with a diamond structure has an even wide and robust photonic gap[22, 103] for an even lower refractive index contrast (n ~ 2). Figure 33 shows the theoretical calculated band diagram for a diamond structure (refractive index contrast is 3.6). A complete photonic bandgap exists and the center wavelength is at approximately $a/0.47$. Compared with the common inverse opals, the photonic bandgap of the diamond structure is much wider and more robust. For dielectric spheres (n=3.6) and air voids, a maximum gap to midgap ratio ($\Delta w/w_g$) of 15.7% is found, for volume filling ratio (f) of 37%. Volume filling ratio is the volume of dielectric material divided by the air volume in a unit cell. Conversely, for the case of air spheres and dielectric filling, $\Delta w/w_g$ can reach 28.8% at f =81%. However, standard self-colloidal method could not produced a stable diamond structure because of the low filling fraction (36%) occupied by the colloids [104]. In a painstaking experiment, nano-robotic attached to a SEM was used to pick and place single microspheres into designated location of the diamond structure. Figure 33(b) shows the SEM image of 6 layers of diamond colloidal crystal after long and tedious micro-fabrication process [105].

A proposed method of assembling colloidal microspheres into diamond structure is through ionic colloidal crystallization (ICC). From Makaly's ICC phase diagram, a Wurtzite structure can be achieved from ICC, figure 34(b), by controlling the microspheres' surface charges and ionic strength of the solvent. Using the same dielectric material for the positively and negatively charged spheres, a Wurtzite can be translated into a diamond structure, figure 34(d). More research works have to been carried out to find out the optimal conditions of Wurtzite growth.
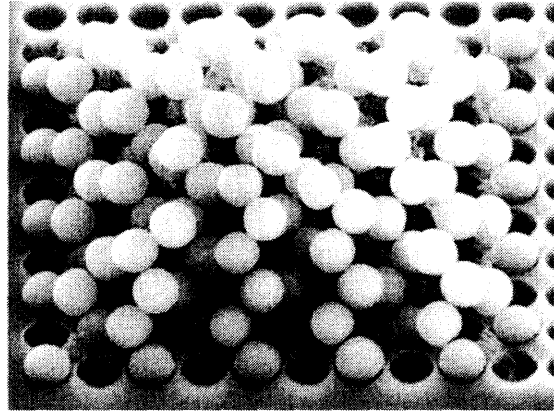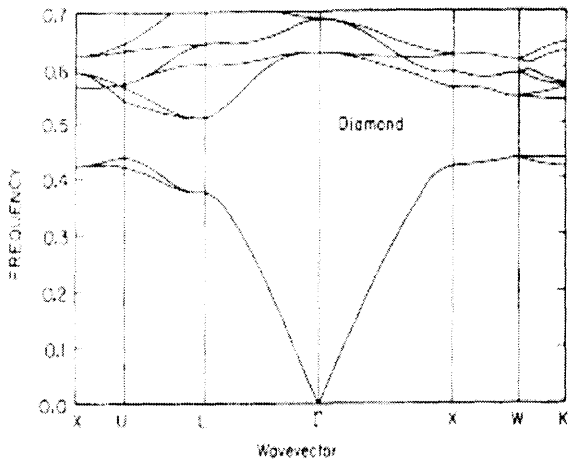
Figure 33. Colloidal crystal diamond lattice. (a) Band diagram exhibits a full photonic bandgap (refractive index contrast is 3.6). (b) Diamond lattice of silica spheres using nano-robotic pick and place (6 layers).
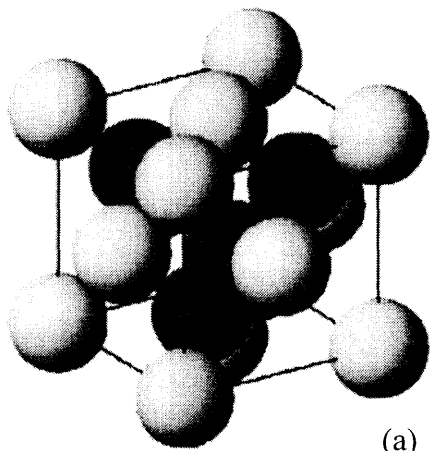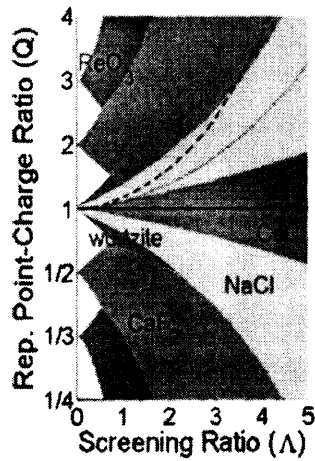
Figure 34. Diamond structure through ICC. (a) A colloidal representation of a diamond structure. (b) ICC Phase diagram, (c) Picture of a Wurtizte structure. (d) Diamond structure.
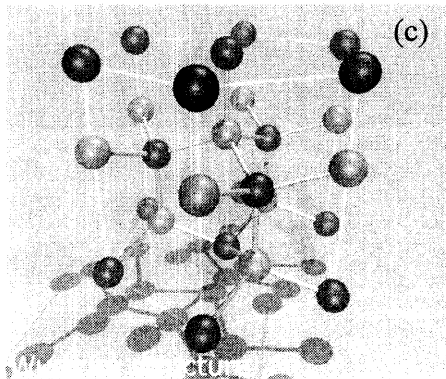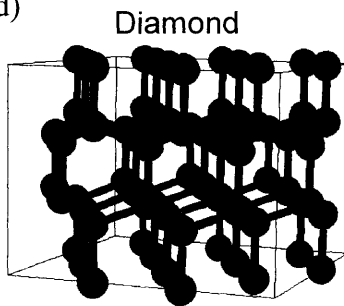
4.5.2 Photonic Integrated Circuit Chip

Waveguide is one of the important components in a photonic or all-optical integrated circuit chip which has attracted huge interest in research. This had created a microphotonic discipline, which focuses on the use semiconductor technology[106] and photonic crystal technology for the implementation of the promising all-optical integrated circuit. Waveguides are analogous to the veins of a body, carrying huge amount of light signals between computational blocks in a chip. Since waveguide would occupy the most chip area, it is crucial that it is compact and has minimal signal cross-talk between one another. This is especially so for large number of waveguides are expected in a Dense Wavelength Division Mutiplexer (DWDM) system.

A 2D top-down microphotonic waveguide has the lowest degree of processing difficulty and this structure generated a lot of research activities. This 2D waveguide has a silicon strip structure on insulator and air space on both sides, figure 35(a). However, there is an intrinsic leakage of electromagnetic waves in the vertical direction. Signal to these structures is limited to traverse mode or a converter is needed at the front stage to convert any out-of-plane signal into traverse mode. The typical propagation loss is 300dB/cm[107] and for micro-scale chip the loss is acceptable. The current state-of the-art Silicon on Insulator (SOI) waveguide achieves a propagation loss 3.6±0.1dB/cm for the Traverse Electric (TE) polarization by smoothing the sidewalls[108], which are the cause of scattering loss.

top

side →

a   400 nm

b
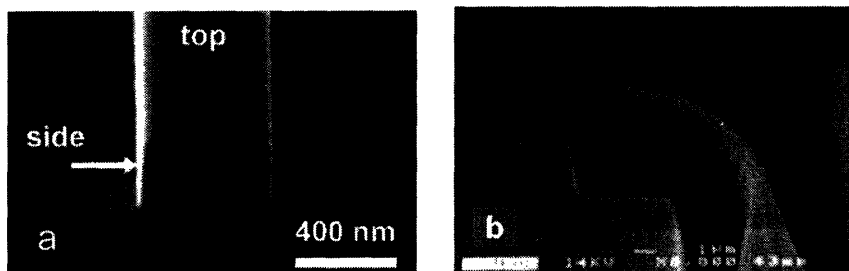
Figure 35.
Components for all-optical IC chip. (a) A strip SOI waveguide, (b) Air trench bend.

Another important interconnect component is a right-angle turn or a band. Figure 35(b) shows a tilted SEM image of an air trench bend with a bending radius of 10.7μm.

This bend structure is made up of Silicon Oxynitride (SiON) thin film material. Such tight bending radius pushes forward the goal of all-optical micro-chip. The propagation loss is 0.1dB/cm[109], an impressive research achievement.

An even lower propagation loss can be achieved in a top-down 2D photonic crystal waveguide. This is a SOI device consisting of a silicon photonic crystal slab with SiO2 lower cladding layers. As shown in figure 36(c), the photonic crystal contains a line of missing 'holes' which is the waveguide. The propagation loss is 1.5dB/mm[110].
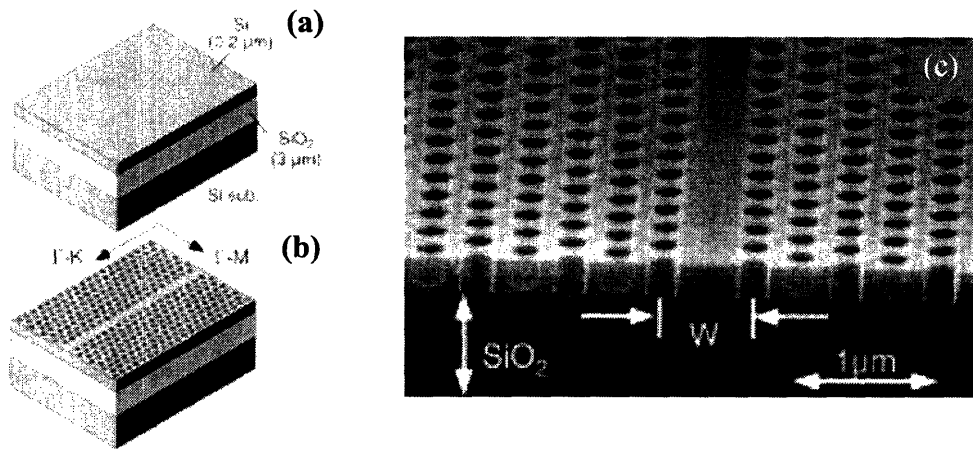
Figure 36. Top-down 2D photonic crystal waveguide. (a) Diagram of a Silicon on Insulator (SOI) substrate, (b)&(c) Diagram and SEM image of a 2D silicon photonic crystal slab with a line defect.
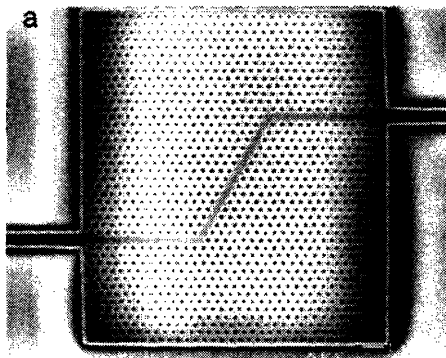
Figure 37. Top SEM view of a double-bend device (two 60° bends)

Building on the success of the top-down photonic crystal slab waveguide structure, a high efficient 60° bend is demonstrated. Figure 37 shows a SEM image of a double-bend

waveguide used in the bending efficiency experiment. A near 100% bending efficiency is observed at certain frequencies at the edge of the photonic bandgap[111] (near the valence band edge). The bending radius is 1 μm at a wavelength of 1.55 μm.

A top-down photonic crystal drop filter[112] was demonstrated and it could be adopted for use in optical multiplexing. Figure 38(a) shows the schematic for drop filter operation. A signal with multiple frequency components or channels is fed into the Bus waveguide. One of the frequency components could be extracted by designing the optical resonator to match the frequency of that desired channels. In resonance, the desired channel is 'dropped' and ceased to exist in the Bus waveguide, it will appear on the Drop waveguide. Consequently, the desired channel can be extracted on the Drop waveguide and this drop filter behaves as a demultiplexer.
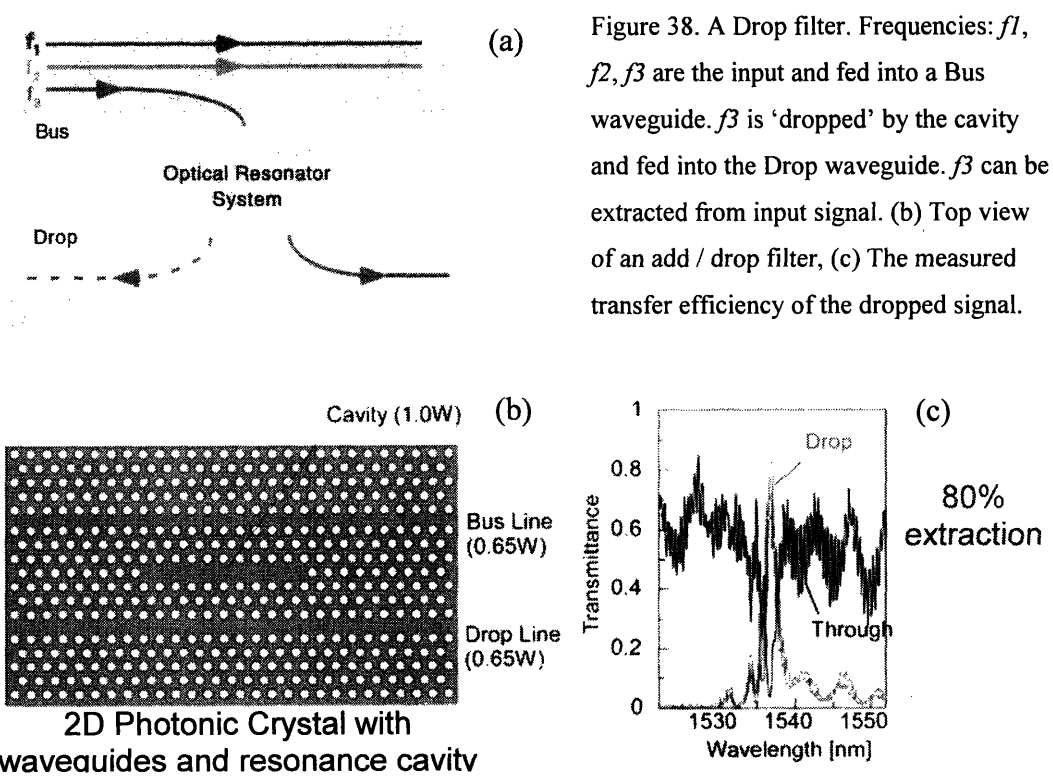
Figure 38. A Drop filter. Frequencies: $f1$, $f2$, $f3$ are the input and fed into a Bus waveguide. $f3$ is 'dropped' by the cavity and fed into the Drop waveguide. $f3$ can be extracted from input signal. (b) Top view of an add / drop filter, (c) The measured transfer efficiency of the dropped signal.

This demultiplexer structure on a single chip is useful for extract a single desired wavelength from a DWDM signal. The DWDM signal is fed into the Bus waveguide as shown in figure 38(b). A desired single wavelength (channel) can be extracted from the

DWDM signal by tailoring the geometries of the drop filter. The desired wavelength is then transferred from the Bus to either in the forward or backward propagation direction of the Drop waveguide. It was shown that cross talk between the bus and the drop for all other frequencies was suppressed. Proving the add/drop filter theory on a physical photonic crystal material, Notomi et al[113] fabricated waveguides, resonators and coupling components in a two-dimensional photonic crystal slabs. This device was built on a Silicon on Insoulator (SOI) photonic crystal slabs with SiO_2 lower cladding layers. Figure 38(b) shows the design of their 4-port channel drop filter, the resonator is a short line-defect with a width of 1.0 W and the Bus/Drop lines with a width of 0.65 W. The width dimension is closely related to the signal wavelength of interest. The measured transmission spectra show that dropping efficiency is approximately 80%, figure 38(c). The photonic crystal is subject to fabrication introduced defects and manifested as light scattering or signal attenuation[114].

A three-dimensional photonic crystal that exhibits a complete photonic bandgap can avoid out-of-plane radiation loss[115]. Figure 39 illustrates a woodpile photonic crystal with an air line defect in the center of the 3D structure. Through simulation, single-mode transmission is supported in the stacked-bar structure by removing one stripe. Signal confinement is improved tremendously and there is no intrinsic signal leakage in the vertical direction[116]. On implementing a woodpile bend structure, strip is removed from a stack and another perpendicular strip is removed from the stack underneath. Signal transmission through the bend is computed to be approximately 95%. The bending efficiency is less than a 2D structure and need to be improved on. Further, the top-down processing steps for stacking structure are tedious and fabrication cost is high.

Self-assembly of colloidal crystal has the potential to offer a simpler and cost-effective approach to create a 3D waveguide structure. It is a compromise between the 2D and 3D top-down waveguide structures 117 as shown in figure 40. The array of colloidal spheres can be etched away using photolithography/etching, electron-beam lithography or multi-photon polymerization as explained in the previous section The array of missing spheres is then filled with a resist and the crystallization is carried out on top. Next, the resist is then etched away and the opal is sintered to create necking between spheres. Germanium (n = 4.1) film is deposited on the opal. The opal template is removed by

calcinations or wet etch. Finally the filled channel can be etched away, leaving behind a chain of air spheres, refer to figure 40. The waveguide is a chain of air spheres in the center of an inverted germanium-shell opal.
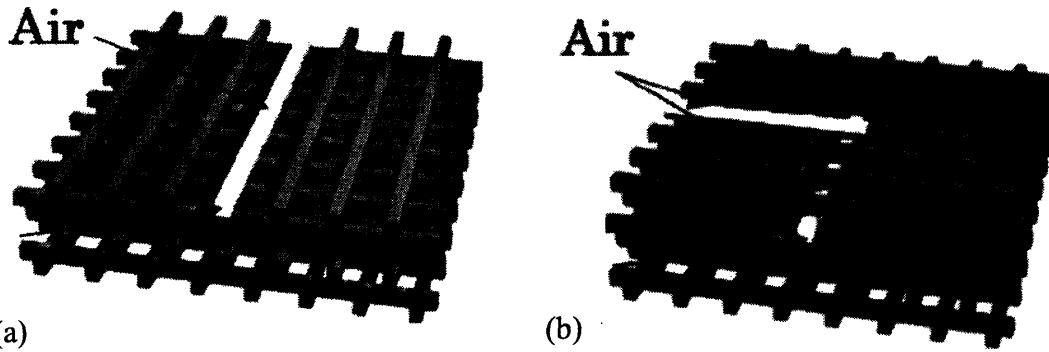
Figure 39. (a) A 3D Woodpile Photonic Crystal waveguide with a line defect. The photonic crystal continues to pile above the line defect to confine electromagnetic wave. (b) Sharp bend crossing adjacent layers.
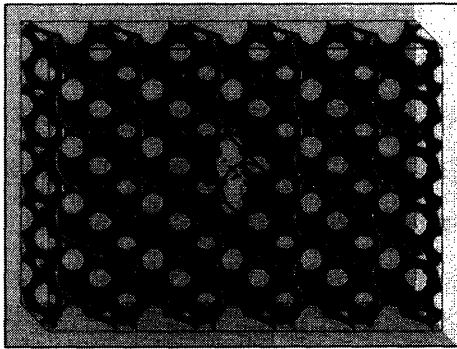
Figure 40. A waveguide made up of array of missing air spheres in the center of an inverted germanium-shell opal.

The inverted germanium opal has a complete photonic bandgap between the 8th and 9th band since n > 2.8. The bandgap reflects electromagnetic wave coming in any directions as long as the wavelength is within the bandgap. An electromagnetic wave of frequency within this bandgap is able to travel along the chain of spheres due to multiple reflections as it propagates. This is analogous to light travelling in an optic fiber due to total internal reflection. Through computer simulation, the chain of air sphere through a inverted Ge-shell opal creates a localized mode in the bandgap between the 392th and

56

393th band[117]. The localized mode supports wave propagation. Further, there is no surface mode found for a chain of air spheres line defects. The absence of surface modes suggests the waveguide should exhibit a very low propagation loss[118]. However, the performance is still limited by intrinsic defects. Finally, it is found that the structure can be optimized to achieve a bandwidth of 113 nm at 1.5 um wavelength through air sphere size optimization.
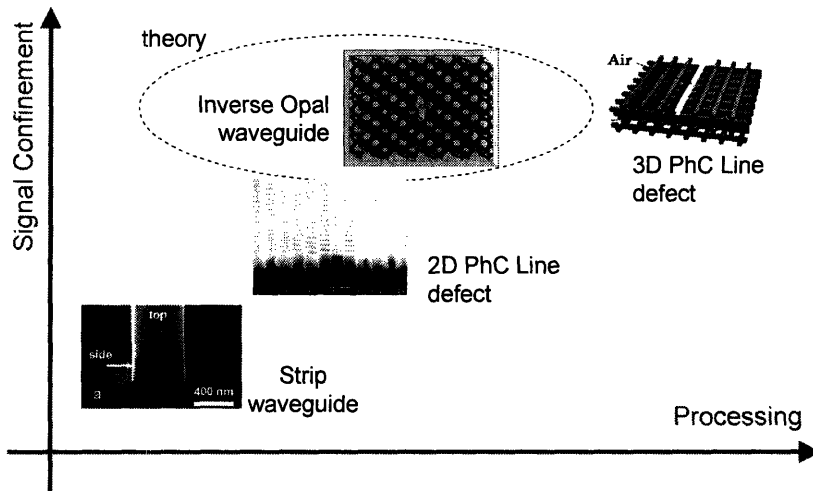
Figure 41. A comparison of level of signal confinement and processing level for strip waveguide, top-down 2D, 3D PhC waveguides and inverse opal waveguide.

Figure 41 illustrated a plot of the level of signal confinement in the various waveguides discussed previously and the degree of processing level required to fabricate them. Both the 2D structures are low in signal confinement and low in the fabrication difficulty. On the other hand, the 3D woodpile waveguide structure shows superior signal confinement capability, but the processing steps are more complicated. A single stack woodpile structure needs thin film deposition, pattern & etch, thin film deposition again, chemical-mechanical polishing (CMP) to smoothen surface and the cycle repeats for multiple stacks. The inverse opal waveguide offers a compromise between the two extremes, giving a relatively higher signal confinement and lower processing requirement. The inverse opal waveguide device need a lithography and etch step in between two colloidal self-assembly processes. Hence, a channel making up of a chain of air spheres can be enclosed in a 3D structure. Finally, the opal undergoes an infiltration procedure to transform into an inverted opal with a complete photonic bandgap with a localized mode.

57

In order to realise a photonic integrated circuit chip, several monolithic components are needed besides a waveguide. They are filters, switches, modulators, resonators, bends and lasers. These consist of passive and active functional blocks that control the flow of light (signals) in a photonic integrated circuit. A photonic integrated circuit chip is only good if there is an interface to the outside world. Looking at its input and output, a photonic integrated circuit is fed by an optics fiber and the manipulated signal exits through an optics fiber eventually. A fiber-to-waveguide is the essential part of a photonic integrated circuit system. In microphotonic, there is a fiber-to-waveguide (and vice versa) coupler solution and it was reported to have an insertion loss of 1.9dB at wavelength 1.54μm, figure 42.

The research in top-down type of photonic devices has progressed far as can be seen in figure 42. Today, much of colloidal integrated circuit specific devices are still in infancy stage, there is a lot of considerations on the pursue of the colloidal integrated circuit. The discussion on the disorder in section 4.3 has shown that the optical performance of an inverse opal waveguide is still limited by the intrinsic defects form during growth. As a conclusion, the colloidal photonic crystal should be pursue as a bulk photonic crystal application (for example: reflectors, optical switch, bio-sensor), which was shown that it is inherently robust against stacking disorder, cracks and voids. The following section discusses some example of bulk photonic crystal product and other non-photonic applications.

SOI propagation
loss =
3.6±0.1dB/cm

Waveguide in a 3D
Inverted Opal
(theory).

Graded Index
Coupler
loss = 1.9dB
@ λ = 1.54µm

No equivalent
currently

PhC notch filter ,
high measured Q
factor (~265)

Not planar version
currently

Add / drop filter ,
80% extraction
efficiency

No equivalent
currently

Top-down Photonic Devices   Bottom-up Photonic Devices
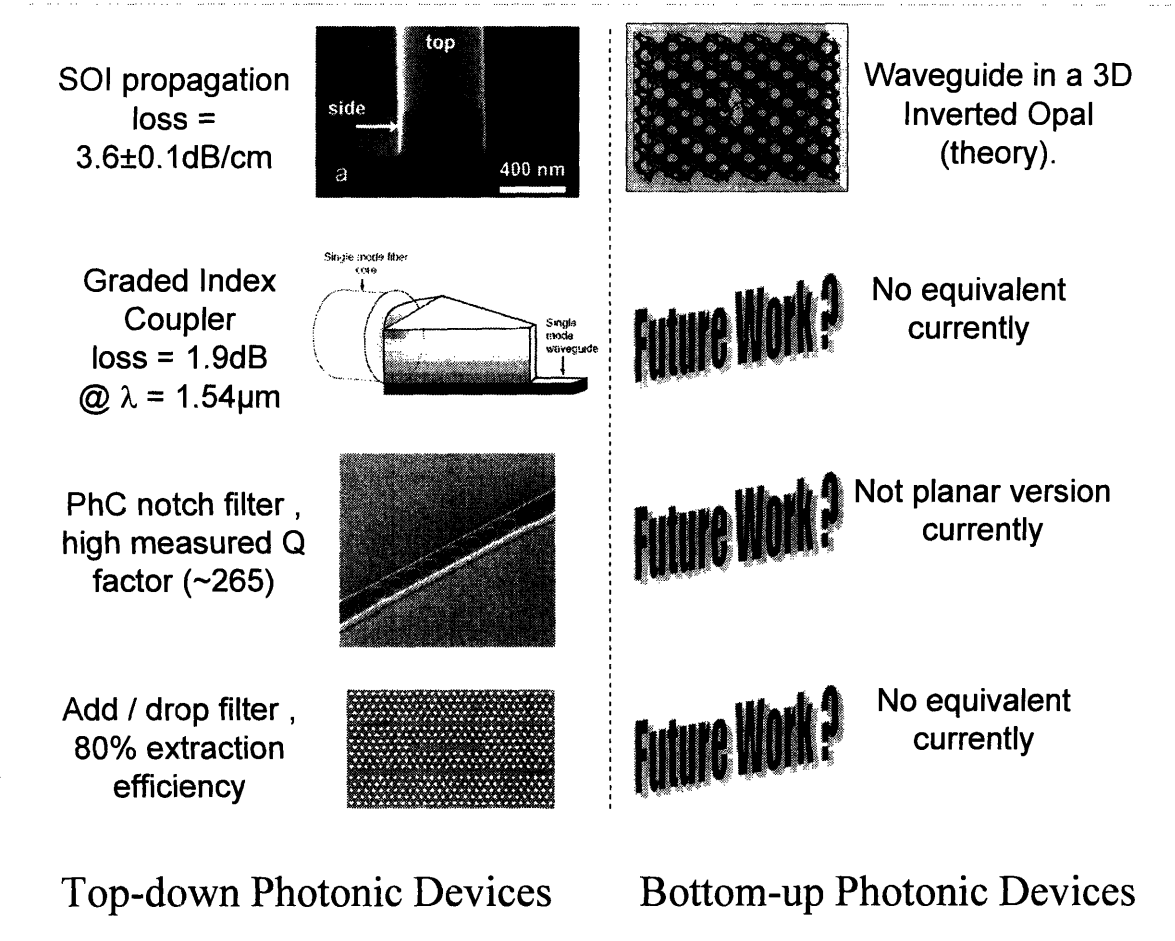
Figure 42. A comparison of the progress between top-down and bottom up photonic device.

4.5.3 Optically Excited ZnO Laser

In the recent years, Zinc oxide (ZnO) has generated a huge interest in research due to the potential use of ZnO for blue lasers and also as a transparent conductive electrode in thin film solar cells and flat panel displays[119]. ZnO has a wide, direct electronic band gap (3.3 eV). With a shorter wavelength emission, it is ideal for blue and ultraviolet spectral semiconductor lasers. Potentially, ZnO laser can find applications in high-density optical data storage.

In additional, ZnO materials are ideal for making microelectronic devices. Since ZnO has wide band gap, it minimizes the leakage currents due to thermal variation in microelectronic devices. Other properties of ZnO include: high chemical and thermal stability, large mechanical strength and large piezoelectric coefficients[120].

The main advantage of ZnO is its high binding energy of the free exciton. The binding energy of the free exciton is about 60 meV at room temperature. A high binding energy of exciton enables one to realize room temperature excitonic devices. For example, good exciton devices have superior photoluminescence property[121]. Hence, ZnO is an efficient emission material at near-UV wavelengths.

ZnO infiltrated into a colloidal crystal is investigated for any novel photonic crystal applications[122]. Here, ZnO was infiltrated into polystyrene (PS) colloidal crystal template by chemical vapor deposition (CVD). Next, the PS microspheres were removed by calcinations and the final structure is a ZnO inverted opal. ZnO has a refractive index ranges from 1.9 through 2.2. A pseudo gap can still be achieved for the ZnO inverse opal and approximately 40% reflectance can be achieved, figure 43.

In a lasing experiment, the ZnO inverse opal [111] surface is optically pumped by a white light source with variable wavelength[123]. Figure 43 shows the reflection spectral and lasing emission for various microspheres' sizes. In the figure, indicator *R1*, *R2* and *R3* correspond to the first order Bragg peak, second main peak, and the third main peak respectively. Indicator *L* corresponds to laser emission peak. The laser emissions peak at near-UV spectrum. The authors suggested that the lasing mode occur at the higher order flat band region where the group velocity is abnormally low. The reduced group velocity helps in confine light effectively and it enhances emission. The emission width of lasing

peaks ranges from 0.1 – 0.3 nm, exhibiting strong delta function. The output beam is highly directional with divergence angle of 6°.
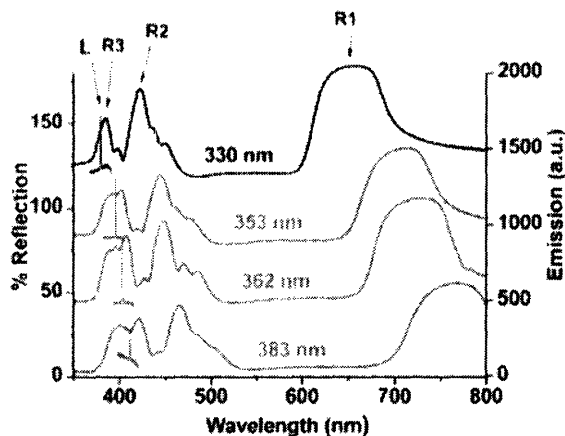
Figure 43. Reflection and lasing spectra of ZnO inverted opals for microspheres' diameter 330, 353, 362 and 383 nm. ZnO inverted opal is optical pumped on the [111] surface. R1, R2, R3 and L correspond to the first order Bragg peak, second main peak, third main peak and emission peak respectively.

The advantage of inverted ZnO opal for laser application over other ZnO laser implementations is the ease of fabrication. These other laser implementations include the growth of ZnO quantum dots that required very precise control. On the other hand, the colloidal crystal offers a periodic template on which ZnO can be deposited on easily. Further, because of the unique flat band characteristic in photonic crystal's band diagram, the low group velocity helps in confining light. Thus, the inverted opal structure becomes a gain medium for lasing. The ultimate goal of the inverted ZnO opal research is to achieve an electrically pumped laser.

ZnO has a piezoelectric property. Potentially, inverted ZnO opal, with its porous scald-fold structure, can be used for sensitive displacement sensor or an electrically driven actuator. This could be an interesting application to explore on. However, the piezoelectric effect of the as-grown amorphous ZnO has to be determined for its effectiveness in sensing and actuation. In an optical switch example, an applied voltage across the inverted ZnO opal causes it to expand and contract due to piezoelectric effect. Consequently, the lattice parameter o f t he i nverse o pal c hanges a nd t hus, t he c hanging b andgap spectral l ocation could allow light to pass or not.

4.5.4 Superprism

Previously, anomalous dispersion characteristic near the band edge or near to flat band was used to slow down the speed of light, improve light confinement in a laser gain medium. This greatly improved on laser emission efficiency. Here, the dispersive nature of certain regions of the band diagram can demonstrate other interesting phenomenon: Superprism effect. Dispersion is simply defined as different wavelengths of light get slow at a different rate due to the refractive index dependence on wavelength. This creates a spatial spread of light into different colors as it enters a dispersive medium at an angle. Kosha et al[124] demonstrated that the dispersion of light in a photonic crystal was 500 times stronger (in their experiment) than the dispersion in conventional prisms, figure 44. Superprism is based on the anomalous dispersion of photonic crystal near band edge or flat band region to control the propagation of light.
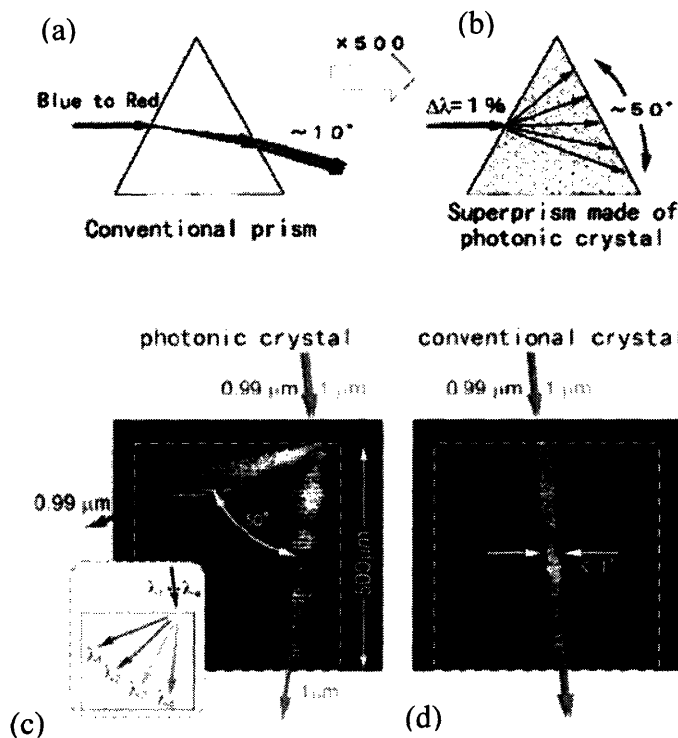
Figure 44. The superprism phenomenon was demonstrated at optical wavelengths in a 2D photonic crystals (PC's) fabricated on Si

Incident light of wavelength falls in the anomalous dispersive region near to flat band or band edge is deflected. The degree of the deflection depends on the dispersion

sensitivity. In another experiment[125], an angular spread of about 10 degree as the incident wavelength is changed from 1290 nm to 1310nm. The angular dispersion is approximately 0.5 degree / nm. In the colloidal crystal superprism study[126], it was found similarly that superprism effect takes place edges of pseudo gap and neat to flat bands regions exist. The superprism effect can find many applications in beam splitter, beam steering, WDM filter and optical de-multiplexer. The only problem is the high loss in output beam intensity that needs to be addressed before useful devices can be realize.

4.5.5 Solar Cell

In 1991, O'Regan et al[127] reported a widely cited paper on the use of dye-sensitized Titanium dioxide (TiO$_2$, titania) film for efficient light harvesting. This is commonly known as Gratzel photoelectrochemical cell. The cell consist of an electrolyte and two electrodes. TiO$_2$ film is grown on the cathode. The TiO$_2$ particles were a few nanometers in size and were coated with a monolayer of charge-transfer dye. Because of the high surface area of the semiconductor film, the sensitized TiO$_2$ showed a promising light-to-electric energy conversion of 12% in diffuse daylight condition. This selling point of this work is in the low cost implementation. The current small scale sample limits in the amount of energy conversion, it is expected to have an even high conversion efficiency for larger cell. In the advent of growing energy cost and demand, this could be the future electricity generator and would be more commercially viable than the present expensive photovoltaic devices.

Dye-sensitized TiO$_2$ inverted opal solar cells are a promising alternative to conventional photovoltaic devices based on p-n junctions[128]. It consists of a highly porous wide-band-gap semiconductor with a liquid ionic conductor. Electrodes connect them to external electric circuit. The dye harvests the solar energy and injects photoexcited electrons into the TiO$_2$ inverted opal. The high porosity of the inverse opal structure gives a high surface area than a laminar device. This helps in the higher charge injection concentration.

The low group velocity near the band edges and flat bands regions help to confine light in an inverse opal material. The inverse opal can be tuned so that it confines the

electromagnetic wave spectral, which can be easily absorbed by the photo-senistive dye. Photo-generated carriers were observed to be higher due to the light confinement property[129]. Further the use of smaller colloidal microspheres (typically with a diameter smaller than 150 nm) causes the formation of photonic band gap in the UV spectra range. Consequently, incident visible light (not reflected by the gap centered in UV spectra range) is able to penetrate the inverse opal and be absorbed by the dye.

On another use of colloidal photonic crystal in solar energy harvesting is trapping light between conventional solar cells. Colloidal photonic crystals have excellent reflection quality and they can be place on both sides of solar cell to bounce light back and forth to improve on energy absorption and efficiency in a solar cell. Colloidal photonic crystal film is inexpensive to process, and they make excellent reflection coating for light trapping in solar cell.

4.5.6 Other Non-Photonic Applications

An inverted opal made up of acrylamide polymer can be used as a humidity sensor [130]. The acrylamide hydrogel is hydrophilic and has excellent water absorption. When the humidity increases, the hydrophilic acrylamide hydrogel absorbs water and undergoes swelling in all direction due to structural change[131]. This swelling causes the spacing between air spheres to increase. By Bragg law, the reflectance spectrum peak shift is a result of the change in the lattice parameter. Observable change in reflectivity starts after about 10 seconds later. Hence, by monitoring the reflectance peak, humidity can be measured.
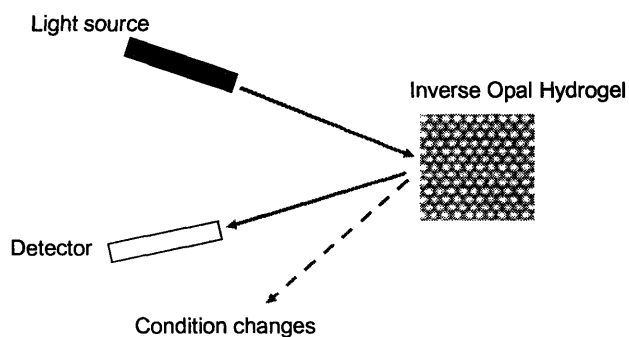
Figure 45. A change in humidity, glucose concentration or pH level leads to the change in lattice spacing. By Bragg's law, the angle of reflection changes. The degree humidity, glucose concentration or pH level can be measured by monitoring in the change of reflection peak

.

An inverted opal made up of glucose-sensitive hydrogel can be used as a glucose sensor[132]. Phenylboronic acid is infiltrated into the voids of the colloidal crystal. The inverse opal forms by a template removal process. The reaction between the phenylboronic acid functional group and the 1,2-cis-diol glucose causes the inverse opal to swell reversibly. Similarly with the previous optical monitoring, glucose can be detected. From experiment, the response time is between 5 to 45 seconds depending on glucose concentration.

An inverted opal made up of pH-sensitive hydrogel is used to implement a pH sensor[133]. The hydrogel is synthesized with a mixture of 2-hydroxyethyl methacrylate (HEMA) and acrylic acid (AA). Like before, the inverted hydrogel opal swells in volume when placed in an ionic solution due to Donnan potential and unexplain polymer-water interaction. Consequently, the pH-sensitive hydrogel invered opal exhibits pH-dependent shift in the reflectivity peak. However, the effect of optical property change takes place in a lengthy 1200 seconds due to slow chemistry equilibrium change. More research works are expected to fine-tune the process.

4.6 Summary of Assessment

The case studies presented thus far are some of the exciting applications of colloidal crystal. The assembling of colloidal particles into ordered structure has generated significant interest because of numerous potential applications that can be derived from the porous template. Other applications that are not covered include the use of monolayer of colloidal crystal film as a non-lithographic nano-scale masks, the 3D porous structure as catalysts, chemical filters and battery electrodes.

Table 1. Advantages and disadvantages of colloidal self-assembly for photonic application

Advatanges	Disadvantage
1. Forms 3D ordered structure naturally. 2. Tailors the lattice parameters and material properties. 3. Fabricates using simple equipment and in parallel. 4. Infiltrates to implement application specific devices.	1. Intrinsic defects are inherent during growth. 2. Light scattering due to defects. 3. FCC colloidal crystal restricts the choice of infiltration material for complete photonic bandgap.

Self-assembly of colloidal crystal is a simpler and low cost method to create a 3D periodic structure. The shortcomings are intrinsic defects such as missing microsphere and cracks in the colloidal crystal are inherent. Such defects are light scatter centers in photonic application and they translate as signal propagation loss, see figure 46. However, all the evidences presented thus far have shown that the photonic bandgap is robust against such defects. Table 1 lists the advantages and disadvantages of colloidal self-assembly for photonic application.

(a) No crack   (b)Cracks
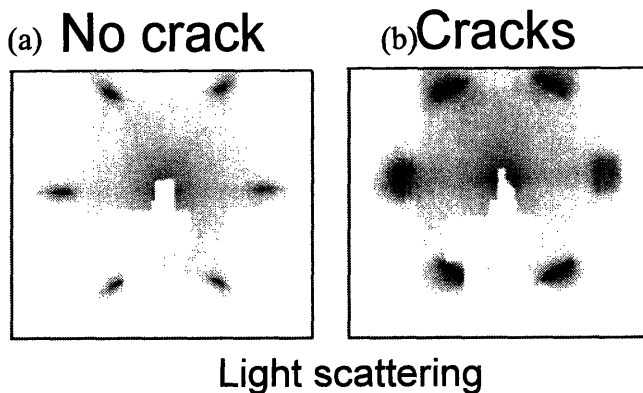
Light scattering

Figure 46. Diffraction experiment demonstrating the effect of light scattering as signal propagation loss. The white objects in pictures are inverse opal sample attached to a holder. The diffraction pattern is in the background. (a) Diffraction pattern is sharp for no crack, (b) diffraction pattern is fuzzy when there is cracks in the inverse opal, due to more light scattering.

Colloidal crystal is best utilized in its bulk form, taking advantage of the ease to form 3D structure under natural process, for example sedimentation. Lithographically defined colloidal crystal device (waveguiding application) adds to the cost of production. In the case of waveguide structure, intrinsic defects in colloidal crystal still limit the transmission capability and further, it will be not cost-competitive to complete with top-down fabricated waveguides. Self-assembly bottom-up method for photonic integrated circuit is in the infancy stage. On the other hand, the research on top-down 2D photonic crystal and silicon micro-photonic devices is pursued for many years and with great result. In the research on photonic integrated circuit, the top-down research has progressed far and many functional blocks are now in place, figure 47. The remaining works to realize a truly top-down all-optical integrated chip are on-chip laser, optical switch and optical modulator (Kerr effect).

Nevertheless, the bulk colloidal crystal or the synthetic opal is attractive option to achieve 3D periodic structure for the study of photonic band structure effects in the infrared, near-infrared, and visible wavelength regimes. In the case studies discussed, the bulk colloidal crystal can turn into application-specific inverse opal by materials infiltration. They are the high-speed optical switch, optically excited laser, solar cell, pH, humidity, glucose sensor and the list can go on limited by imagination. All these are possible due to the favorable attributes or characteristics of an photonic colloidal crystal :

1. Self-assembled (Simple, low cost)
2. Ordered template (PhC, Sensors)
3. Photonic Bandgap (EM wave filter)
4. Dispersive Band edge (superprism)
5. Flat bands or band edges (slow group velocity, light confining)
6. Large surface area (catalyst , semiconductor devices)
7. Large porosity (filter, catalyst)

Top-down Photonic Integrated Circuit
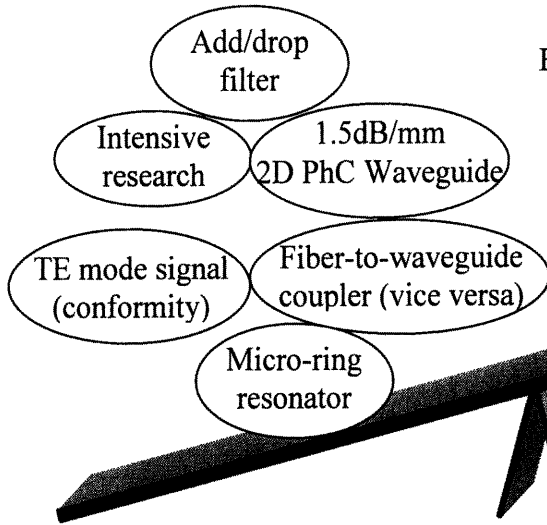
Bottom-up Photonic Integrated Circuit
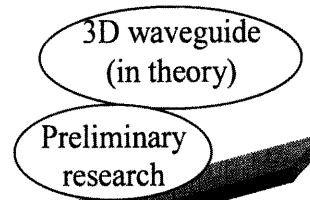
Figure 47. Analysis on the progress and impact of top-down versus bottom-up photonic integrated circuit.

5.0 Cost Analysis : Self-assembly of Colloidal Microspheres

5.1 Market Survey: Photonic components

In a network survey made in 2005[134], it was reported that the photonic industrial has underwent a consolidation phase since 2001, the burst of the Internet bubble. About 75% of the photonic component manufacturers had either merged or closed down. Figure 48 shows the sales of the optical network equipment and optical discrete components for the past 8 years. Years leading up to 2000 saw the great rise in the sales of optical items due to the need for high-speed telecommunication to meet the bandwidth demand for ever increasing Internet's users. After which, the Internet bubble burst and resulted in the dramatically fall in the sale revenue.
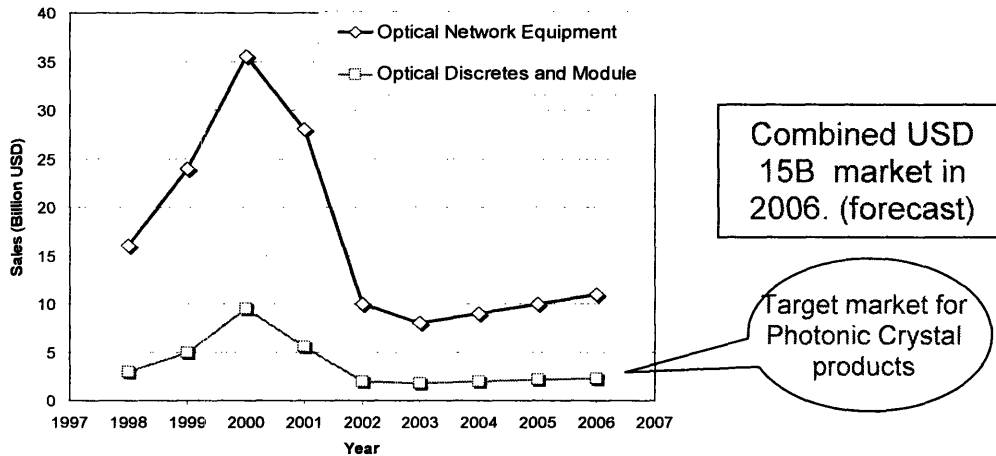
Figure 48. Sales of the optical network equipment and optical discrete components between 1998 through 2005, Communication Technology Roadmap (CTR) 2005.

In the Communication Technology Roadmap (CTR) 2005 report[135] , the 2006 forecast combined sale of the optical network equipment and discrete components is predicted to be in the region of $15 billion. In particular, the target market for optical discrete component is estimated to be $2.5 billon market. Hence, a chunk of this $2.5 billion market could be the potential market for the proposed photonic crystal devices. Further the growth of optical discrete component is expected to reach $5.7 billion by the year 2009 (Average annual growth rate 18.2%). This high growth sector is expected to

boost the demand of optical component, and hence photonic crystal devices are well positioned to capitalize on the forecasted upward trend.

Inverse opal is able to filter out (reflecting) selected band of frequency and transmitting other frequencies. This is ideal replacement for a monochromator, a common optical component that transmits a narrow band of wavelengths of electromagnetic wave. The monochromator can manually select the band of signal by mechanical adjusting the arrangement of gratings and prisms. Hence it can be seen that such devices are bulky and expensive ($20k a piece). The compact opal reflectors can be a great low cost solution.

5.2 Market Survey: Photovoltaic

According to the U.S. Department of Energy, the global photovoltaic market was estimated to about a $4 billion in 2004[136]. The photovoltaic market is expected to grow on an average of 20% to 25% a year due to rising environmental awareness and increased energy needs. On top of it, there is a global shortage[137] of processed silicon for the photovoltaic industries due to competition from the booming semiconductor sector. Novel materials that can potentially replace the silicon material is good news for photovoltaic industries. For example, dye-sensitized titania inverted opal. Colloidal photonic crystal's research in solar cell could alleviate the rising need for alternative energy and silicon material shortage in the future. Figure 49 illustrates the decline trend of photovoltaic price per watt generated and this could be a benchmark for colloidal photonic crystal cost analysis.
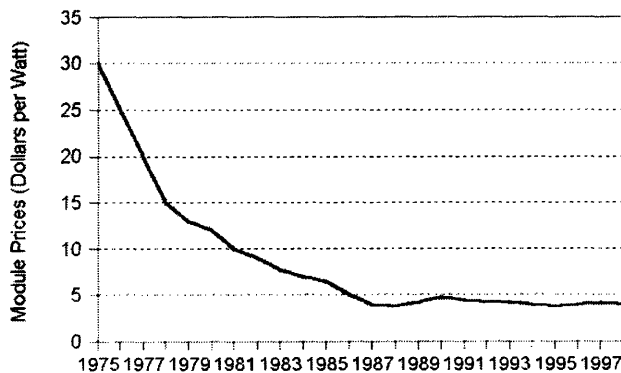
Figure 49. Price of photovoltaic module per watt between 1975 and 1998. Price is expected to be less than $5/watt now.

Source: P Maycock, The World Photovoltaic Market 1975-1998 (Warrenton, VA: PV Energy Systems, Inc., August 1999), p A-3

5.3 Inverse Opal Frabrication Procedures

In this cost analysis, the colloidal crystal template or the synthetic opal is fabricated using widely cited bottom-up method known as the isothermal heating evaporation induced self-assembly (IHEISA[138]). In essence, this is a vertical deposition where heating element is in place to maintain proper temperature control, humidity control and convective flow. As reported, the rapid IHEISA method gave a very high quality silica colloidal crystal film on a substrate.

The crystallization of the colloidal particles on a glass slide is performed in a suspension of silica colloids (500nm diameter) and ethanol in a vial. Before, the glass slides are prepared with Piranha clean for improved adhesion with the colloidal crystal. The vial is placed inside an isothermal ethylene glycol bath and the temperature is kept at 80°C. Convective flow is induced by heating to keep the microspheres suspended at the meniscus while ethanol evaporates. The deposition rate is approximately 2 mm/h. Typically, 5-10 sphere layers film is deposited for silica microsphere concentration of 4-7 wt-% suspension. After dried, the colloidal crystal is sintered to create necks between silica spheres (3hours at 950°C for silica; 5minutes at 105°C for PS). These necks provide links between the microspheres and it enables effective chemical etching of the silica template throughout the crystal.

5.3.1 Infiltration of Silicon through LPCVD

Disilane (Si_2H_6) is a common precursor for depositing poly and amorphous silicon (Si) films in a LPCVD. Here, this method is used to infiltrate the synthetic opal in order to create a silicon inverse opal[139], following by a calcinations process. Here, the cost of setting up the LPCVD process and the deposition of silicon are modeled. Since the growth recipe is not commonly disclosed in the literature, the effort here is to get an estimated cost of filling the voids of an opal using silicon through systematic steps.

From a paper describing the LPCVD process[140], the reported growth specification is: 150 angstrom/min of Si, 500°C, disilane 2.5 sccm, 1 torr. To convert the Si_2H_6 flow rate

in term of weight per unit time, the density of Si_2H_6 has to be determined. The idea gas law is employed to calculate the molar volume of Si_2H_6. The assumption of an ideal gas is nearly valid due to the LPCVD is a relatively low pressure and high temperature process. Consequently, the molecules are wide apart and the ideal gas assumption is appropriate. Since, the standard flow rate of disilane is given (STP: 273k, 1atm), to conform to this standard, the molar volume is

$$\bar{\upsilon} = \frac{RT}{P}$$

$$= \frac{0.08205 \frac{L \cdot atm}{k \cdot mol} \times (273k)}{1 atm}$$

$$= 2.23 \times 10^4 \, cm^3 / mol$$

where R, T and P is ideal gas constant, temperature and pressure respectively.

The density is the molecular mass of Si_2H_6 (62.22g) divided by the molar volume:

$$\rho = \frac{62.22 g / mol}{2.23 \times 10^4 cm^3 / mol}$$

$$= 2.79 \times 10^{-3} g / cm^{-3}$$

To convert the flow rate into weight per unit time:

$$Flowrate = 2.5 sccm$$

$$= 2.5 cm^{-3} / min \quad \times \quad 2.79 \times 10^{-3} g / cm^{-3}$$

$$= 6.98 \times 10^{-3} g / min$$

From simulation, the maximum photonic bandgap can be obtained when there is about 90% - 97% of void filling, leaving interstitial air voids between the colloidal microspheres[139]. Further, Blanco et al had shown that an 88% infiltration of Si into available opal template voids could result in a reasonably wide bandgap[139]. In this cost analysis, 100% infiltration of voids is targeted for ease in calculation. Figure 50(a) shows (100) surface of a synthetic opal and the resulting infiltrated structure after calcination. It can be shown that the air void in (100) plane is the largest and the dimension is determined

72

next for the worst-case deposition duration needed. Other planes are observed to have smaller air voids.
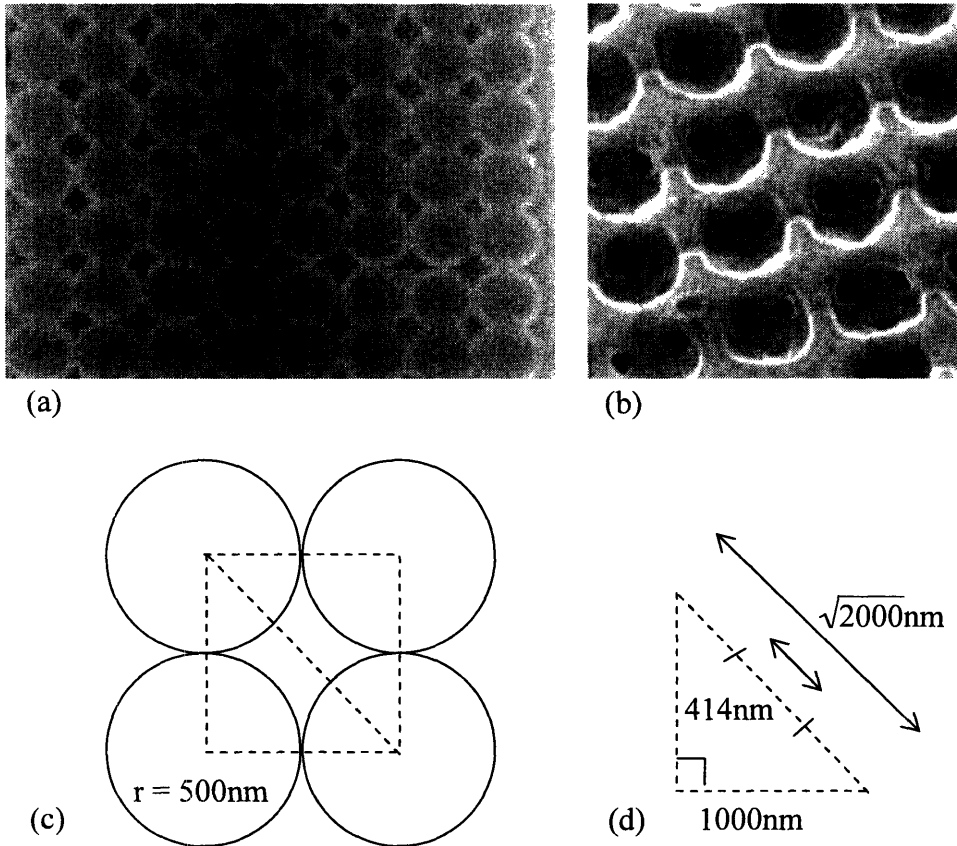
Figure 50. (a) The SEM image of the (100) surface of a synthetic opal, the microspheres have an average 500nm diameter. (b) The air voids are infiltrated with silicon and the colloidal microspheres are etched away. The final structure is an inverse opal with silicon matrix and air spheres. (c) A diagram of hard spheres in contact without the annealing process. This approach gives the largest possible air void dimension. (d) The air voids have an average of 414nm in length.

As shown in figure 50(d), an average length of 414nm air void has to be filled by the LPCVD process assuming no sintering process. Since LPCVD infiltration is an isotopic deposition process[141], the deposition of silicon on the colloidal microspheres is about half of 414nm thick. Adding a safety margin to the deposition, the required silicon deposition would be 400nm layer thick for 500nm diameter colloidal particles. This would be sufficient to infiltrate all air voids at all planes of the synthetic opal. For a growth rate of 150angstorm/min, total time is estimated to be 30min (=400/15). Because the growth

parameters[140] are for thin film growth, a safety margin of thrice the length of duration is added to ensure the 3D voids are completely filled. Total time of LPCVD is planned for 120min. Next, the silica template is etched away using 1 wt-% of hydrofluoric acid (HF) aqueous solution.

5.3.2 Infiltration of Silica through Sol Gel

The synthetic opal (Polystylene microsphere) is deposited and sintered similarly as before. The opal is infiltrated with Silica sol[142]. The silica sol is made up of tetraethyl orthosilicate, ethanol, and HCl solution. The sol is stirred for 4 hours and is poured over the opal template next. The sample is let dry for 12 hours. Finally the opal is calcined at 500 °C for 6 h to decompose the PS microspheres.

5.3.3 Infiltration of Zinc Oxide by Chemical Deposition

The colloidal crystal (silica microsphere) is deposited and sintered similarly as before. The colloidal crystal template is infiltrated using chemical deposition of Zinc Nitrate Hexahydrate ($Zn(NO_3)_2 \cdot 6H_2O$) solution[143]. The deposition is carried out in a thermal bath at 60 °C for 1.5 hour. After which, the samples were heated in a furnace at 550 °C for 2 hours. This is to decompose the zinc nitrate into zinc oxide. The deposition step is carried out for several times and the weight of the sample is checked after the heat treatment. The whole process ends when there is very little incremental gain in weight. Hence, the voids are said to be fully filled.

5.4 Cost Analysis for Inverse Opal Fabrication

Based on the fabrication procedures outlined above, the cost of the material and equipment used in a laboratory setting are computed for the inverted silicon, silica and zinc oxide opals. These opaline materials are frequently quoted in many published papers for the studies in photonic bandgap and optical properties. The unit cost of raw materials and the retail price of equipment are sourced from fellow colleague[144], Aldrich Online Shopping Web and internet search result. The cost of equipment is computed from a linear annual depreciation cost from it predicted useful life. Appendix 1-3 listed the fabrication procedures and cost clearly. The batch size for the fabrication is 10 glass slides (3" by 1"). The equipment used in the cost assessment are the Furnace, Thermal Bath, Mixer, Low Pressure Chemical Vapor Deposition (LPCVD) and the consumables.

The breakdown of the fabrication cost in a laboratory for a 1" by 1" sample is

Table 2. Summary of cost (Appendix 1-3) (1" × 1" sample)

Inverse opal material	Infiltration method	Material Cost ($)	Equipment Cost ($)	Total Cost ($)
Silicon	LPCVD	7.91	0.44	8.35
Silica	Sol Gel	5.87	0.21	6.08
Zinc Oxide	Chemical Deposition	3.62	0.27	3.89

As shown in the appendix, the cost of preparing synthetic opal is roughly the same for all the three different materials infiltration. For the case: inverted silicon opal, it is made by the infiltration of disilane gas in a LPCVD process. Comparing with silica and ZnO total cost, the inverted silicon opal is a more costly product in this assessment. This is partly because the silicon infiltration uses a LPCVD, which is a costly equipment. On the other hand, silica and ZnO uses sol gel and chemical deposition infiltration process respectively with no complicated tool.

To do a quick incremental cost model of implementing lithographically-defined colloidal photonic devices, such as an inverse opal waveguide, the cost of the

photolithography system or the electron-beam lithography can be added to the figures above. The cost of equipment and usual cost per batch run are computed in appendix 2. Photolithography system[145] is estimated to be $10M for resolution 0.25μm and the mask is estimated to be $15k. Production is estimated to be 45min per batch, and total number of 10000 batches is used to account for the mask cost. Besides, the photoresist and etching cost are estimated is the cost analysis. Meanwhile, the electron-beam lithography[146] is estimated to be $6M for resolution 0.25μm and it is a maskless process. Production is longer due to serial scanning and it is estimated to be 3 hour per batch.

From appendix 4, the incremental costs of lithography equipment for a 1" by 1" sample are

Table 3. Summary of equipment cost (Appendix 4) (1" × 1" sample)

Equipment	Cost ($)
Photolithography system	4.35
Electron-beam lithography	7.18

As listed in table 3, the incremental cost of using lithography equipment is about 10 to 35 times higher than the equipment cost in table 2. For the total cost, the material cost is expected to raise due to the additional crystallization procedures following the lithography/etching. The total cost of creating extrinsic defects in an inverse opal device for 1" by 1" sample is estimated to be:

Table 4. Estimated cost of patterning the inverse opal (1" × 1" sample).

Description	Cost ($)
Waveguide in a inverse opal (1" by 1" glass substrate)	$10 to $20

Taking the averages of table 2 and table 4, the average cost of fabricating bulk and patterned inverse opal in a laboratory is estimated to be:

Table 5. Estimated cost bulk and patterened inverse opal (1" × 1" sample).

Description	Average Cost ($)
Bulk inverse opal	$6
Patterned inverse opal	$15

From table 5, the cost of making patterned inverse opal is more than twice to that of bulk inverse opal. Moreover it was shown earlier that the optical properties of such lithographically patterned inverse opal devices are limited by the intrinsic defects.

The cost assessment is based laboratory techniques on the technical papers published in international journals. They are not necessarily the optimized techniques for the most cost effective way of producing inverse opals. Nevertheless, the cost figure gives a guide on the continual optimization in cost, time and fabrication technique in the future. The bulk of the cost lies in the material and it should be optimized for cost effectiveness. The actual cost for industrial optimized processes would probably cut down 50 ~ 70 % on the laboratory work due to economies of scale and higher efficiency. In the advent of soft-lithography, the cost of fabricating patterned inverse opal may reduce due to use of simple and less costly tools.

5.5 Cost Analysis for Top-down 2D Photonic Crystal Fabrication

Liegl et al[147] discussed on a typical microelectronic fabrication cost. For feature size 0.19μm of 8" wafer technology, the total cost per wafer is $19.20 (memory chip). Taking into consideration of that in a photonic crystal device, there is less processing steps required because metallization, via interconnects, high-quality gate oxide and the like are not required. On the other hand, the bulk of the cost lies in the need for advanced interference lithography to give high-quality ordered dielectric structure for photonic crystal. Besides, the volume of photonic crystal devices is expected to be much lower than the production of memory chips, which are ubiquitous in digital products. Since the photonic crystal devices are not expected to enjoy much of the economies of scale, their

manufacturing cost would be higher. Hence, the cost of manufacturing is estimated to be $80 per 8" wafer. Table 6 shows the estimation of the overall cost per 1" by 1" sample in an industrial production setting.

Table 6. Microelectronic manufacturing cost analysis

Description	Estimate Cost ($)
Front end fabrication (per 8" wafer)	$80.00
1" by 1" die (assume 40 dice after yield loss)	$2.00

The manufacturing of top-down 2D photonic crystal is estimated to be $2.00 per 1" by 1" sample. This exercise approximates the real industrial cost as much as possible. This gives a rough guide on how the manufacturing cost of colloidal photonic crystal need to be in order to complete with the top-down photonic crystal commercially.

Colloidal self-assembly can be proposed as a Low-Cost Micro-fabrication model to create bulk photonic devices. The micro-fabrication work can be carried out in a regular laboratory work space. Clean room facility is not needed to carry out micro- or nano-scale device fabrication. Using simple bench-top chemistry, colloids of wide range of sizes can be synthesized using low cost equipment. For topological confinement of colloidal particles, templated substrate, using soft lithography[42], can be implemented for colloidal self-assembly.

6.0 Conclusion

Photonic crystals has a unique property in which ranges of electromagnetic wave is prohibited to propagate. By tailoring the structure of the photonic crystal, the flow of light can be molded. Colloidal crystal is investigated and assessed for implementation as a photonic crystal.

The self-assembly of colloidal particles into synthetic opal is spontaneous and it can be aided by many techniques such as electrophoresis, topological confinement and ionic colloidal crystallization. The synthetic opal has a close-packed ordered structure and can be use as a template for fabricating a colloidal photonic crystal or commonly known as inverse opal. An inverted silicon opal has a complete photonic bandgap and is suitable to form a waveguiding structure by a lithographically and etching process. The goal is to achieve a photonic integrated circuit made by inverse opal. However, the analysis shows that it is more technically and commercially viable to implement bulk colloidal photonic crystal applications rather than lithographically-defined types. This is because its optical performance is limited by intrinsic defects and the strong competition with existing top-down micro-photonic devices.

The use of bulk inverse opal structures shows promising results for implementing other applications. The bulk inverse opal is inherently robust against stacking disorder, cracks and voids. Potentially, they are useful for implementation in areas of where the unique characteristics of photonic crystal could be capitalized. High reflectivity due to photonic bandgap (reflector), spatial spread of light due to dispersive bands (superprism), slow group velocity due to flat bad (light confinement) and high porosity material (catalyst or chemical filter). In cost analysis of a 1" by 1" sample, the estimated cost of making bulk and lithographically-patterned inverse opal is $6 and $15 respectively in a laboratory. With data from industrial sector, the estimated cost for a top-down fabricated micro-photonic is $2. If carried out commercially, the fabrication cost of inverse opal material can be optimized to meet the competition of top-down photonic micro-photonic devices. In a market survey, the low-cost and versatile inverse opals are well-positioned to challenge existing mechanical optics components and address the raw material shortage in photovoltaic industries.

Appendix 1A: Fabrication of Inverted <u>Silicon</u> Opal (material cost)

No	Description	Unit Cost ($)	Batch Cost ($)

1 Batch = 10 glass slides (3" by 1")

1 Piranha Clean

Batch clean (400ml H2SO4, 200ml H2O2)

No	Description	Unit Cost ($)	Batch Cost ($)
1a)	Glass slide (75 * 25 * 1mm), 72 pcs, Lab Scientific	3.90	0.54
1b)	Sulphric acid (H2SO4) 95-98%, 258105-6X2.5L (Aldrich)	463.54	12.36
1c)	Hydrogen Peroxide (H2O2) 35%, 1 Gallon ()	150.00	7.93

Batch rinse (3000ml DIW, 50ml Ethanol)

No	Description	Unit Cost ($)	Batch Cost ($)
1d)	Deionized water (DIW), 1000 Gallon	15.00	0.01
1e)	Ethanol, semiconductor grade, 40210-2.5L	121.00	2.42

2 Self-assembly of Silica Colloidal Microspheres

Disperse suspension (0.6ml Silica, 500ml Ethanol): 1 batch

No	Description	Unit Cost ($)	Batch Cost ($)
2a)	Silica spheres (0.5um-1.6um), 15ml	315.82	12.63
2b)	Ethanol, semiconductor grade, 40210-2.5L	121.00	24.20

Thermal bath 80C (300Watt), growth rate 2mm/h
To growth 75mm: Time=37.5h

No	Description	Unit Cost ($)	Batch Cost ($)
2c)	Average Electricity Rate (per kilowatthour)	0.84	9.45

3 Sintering of Silica microspheres

To heat in furnace (1200W) 950C for 3 hours

No	Description	Unit Cost ($)	Batch Cost ($)
3a)	Average Electricity Rate (per kilowatthour)	0.84	3.02

4 Silicon Infiltration by LPCVD (42kW)

Deposit 400nm silicon, growth rate = 150A/min: 1 batch
Silane gas flow rate = 6.98 mg/min
Total depostion time plan = 120min

No	Description	Unit Cost ($)	Batch Cost ($)
4a)	Disilane (SiH4) 99.998%, 10g, 463043-10G (Aldrich)	1500.41	125.67
4b)	Average Electricity Rate (per kilowatthour)	0.84	35.28

5 Silica Template Etch

Etch sample in HF (1 wt-%) : 20g HF, 700g DIW

No	Description	Unit Cost ($)	Batch Cost ($)
5a)	Hydrofluoric acid (HF) 35 wt%, 500g (Aldrich)	92.82	3.71
5b)	Deionized water (DIW), 1000 Gallon	15.00	0.01

Description	Batch Cost ($)
Total batch material / utilty cost	237.23
Material / utilty cost for one glass slide	23.72
Material / utilty cost for 1" by 1" sample	7.91

Appendix 1B: Fabrication of Inverted Silicon Opal (equipment cost)

No	Equipment	Est. Cost ($)	Annual Cost ($)	Cost per batch run ($)
1	LPCVD (Horizontal, CVD Equipment Corp)	300,000.00	30,000.00	6.85
2	Thermal Bath (20 liter, Fisher 15-462-20)	1,235.32	247.06	1.07
3	Furnace (Fisher 10-550-14, 1200W)	2,021.25	404.25	0.14
4	Laboratory consumables			5.00

Note 1
LPCVD is forecast to have 10 years lifespan. Annual cost is linear depreciation.
LPCVD run time is estimated to be 120min per batch

Note 2
Thermal Bath is forecasted to have 5 years lifespan. Annual cost is linear depreciation
Thermal bath run time is estimated to be 38hr per batch

Note 3
Furnace is forecasted to have 5 years lifespan. Annual cost is linear depreciation
Thermal bath run time is estimated to be 3hr per batch

Total cost per batch (10 glass slides) run   13.06

Cost per glass slide (3" by 1 ")   1.31

Cost per 1" by 1" sample   0.44

Reference
1 US gallon = 3.7854118 liter

DI WATER COST SHOULD AVERAGE BETWEEN $10-$15 PER THOUSAND GALLONS
http://quanterion.com/RIAC/Library/Library.asp?ArgVal=21220-003

INDUSTRIAL ETHANOL, synthetic ethanol, fuel ethanol market ...
The Ethanol Market industrial ethanol price premium is 35 cents per gallon,

Electricity Rate Comparison by State
http://www.neo.state.ne.us/statshtml/115.htm

Thermal Bath 300W
http://www.eurotechlabs.com

LPCVD , Power 42kW
http://www.tystar.com/furnace_configuration.htm

http://www.4semi.com/dp/cat/84545/84549/mAllItems.cfm?menuid=m_3_2_2
http://www.labjupiter.com/dp/cat/84529/84533/ilist.cfm?LCI=980&menuid=m_1_1

Appendix 2A: Fabrication of Inverted <u>Silica</u> Opal (material cost)

No	Description	Unit Cost ($)	Batch Cost ($)
	1 Batch = 10 glass slides (3" by 1")		

1 Piranha Clean

No	Description	Unit Cost ($)	Batch Cost ($)
	Batch clean (400ml H2SO4, 200ml H2O2)		
1a)	Glass slide (75 * 25 * 1mm), 72 pcs, Lab Scientific	3.90	0.54
1b)	Sulphric acid (H2SO4) 95-98%, 258105-6X2.5L (Aldrich)	463.54	12.36
1c)	Hydrogen Peroxide (H2O2) 35%, 1 Gallon ()	150.00	7.93
	Batch rinse (3000ml DIW, 50ml Ethanol)		
1d)	Deionized water (DIW), 1000 Gallon	15.00	0.01
1e)	Ethanol, semiconductor grade, 40210-2.5L	121.00	2.42

2 Self-assembly of PS Colloidal Microspheres

No	Description	Unit Cost ($)	Batch Cost ($)
	Disperse suspension (0.6ml Silica, 500ml Ethanol): 1 batch		
2a)	PS spheres (20nm-0.9um), 15ml	357.21	14.29
2b)	Ethanol, semiconductor grade, 40210-2.5L	121.00	24.20
	Thermal bath 80degree (300Watt), growth rate 2mm/h		
	To growth 75mm: Time=37.5h		
2c)	Average Electricity Rate (per kilowatthour)	0.84	9.45

3 Sintering of PS microspheres

No	Description	Unit Cost ($)	Batch Cost ($)
	To heat in furnace (1200W) 105C for 5 min		
3a)	Average Electricity Rate (per kilowatthour)	0.84	0.08

4 Infiltration of Silica

No	Description	Unit Cost ($)	Batch Cost ($)
	Batch fill (50ml Si(OC2H5)4, 50ml, 500ml Ethanol), stir 4hr		
4a)	Tetraethyl orthosilicate Si(OC2H5)4, 333859-100ML (Aldrich)	140.63	70.32
4b)	Hydrochloric acid (HCL), 320331-6X500ML (Aldrich)	250.38	4.17
4c)	Ethanol, semiconductor grade, 40210-2.5L	121.00	24.20
4d)	Average Electricity Rate (per kilowatthour), 60W mixer	0.84	0.20

5 Calcination of PS colloidal microspheres

No	Description	Unit Cost ($)	Batch Cost ($)
	Heat at 500degreeC for 6 hr		
5a)	Average Electricity Rate (per kilowatthour), 1200W furnace	0.84	6.05
	Total cost per batch (10 glass slide) run		176.22
	Cost per glass slide (3" by 1")		17.62
	Cost per 1" by 1" sample		5.87

Appendix 2B: Fabrication of Inverted Silica Opal (material cost)

No	Equipment	Retail Cost ($)	Annual Cost (	Cost per batch run ($)
1	Furnace (Fisher 10-550-14, 1200W)	2,021.25	404.25	0.28
2	Thermal Bath (20 liter, Fisher 15-462-20)	1,235.32	247.06	1.07
3	Mixer (Fisher 14-505-21)	215.4	43.08	0.000327854
4	Laboratory consumables			5.00

Note 1
Furnace is forecast to have 5 years lifespan. Annual cost is linear depreciation.
Furnace run time is estimated to be 6hr per batch

Note 2
Thermal Bath is forecasted to have 5 years lifespan. Annual cost is linear depreciation
Thermal bath run time is estimated to be 38hr per batch

Note 3
Mixer is forecasted to have 5 years lifespan. Annual cost is linear depreciation
Mixer run time is estimated to be 4hr per batch

Total cost per batch run	6.35
Cost per glass slide	0.63
Cost per 1" by 1" sample	0.21

Reference
From planar defect in opal to planar defect in inverse opal
Author(s): Wang LK, Yan QF, Zhao XS
Source: LANGMUIR 22 (8): 3481-3484 APR 11 2006

www.aldrich.com

Appendix 3A: Fabrication of Inverted ZnO Opal (material cost)

No	Description	Unit Cost ($)	Batch Cost

1 Batch = 10 glass slides (3" by 1")

1 Piranha Clean

Batch clean (400ml H2SO4, 200ml H2O2)

No	Description	Unit Cost ($)	Batch Cost
1a)	Glass slide (75 * 25 * 1mm), 72 pcs, Lab Scientific	3.90	0.54
1b)	Sulphric acid (H2SO4) 95-98%, 258105-6X2.5L (Aldrich)	463.54	12.36
1c)	Hydrogen Peroxide (H2O2) 35%, 1 Gallon ()	150.00	7.93

Batch rinse (3000ml DIW, 50ml Ethanol)

No	Description	Unit Cost ($)	Batch Cost
1d)	Deionized water (DIW), 1000 Gallon	15.00	0.01
1e)	Ethanol, semiconductor grade, 40210-2.5L	121.00	2.42

2 Self-assembly of Silica Colloidal Microspheres

Disperse suspension (0.6ml Silica, 500ml Ethanol): 1 batch

No	Description	Unit Cost ($)	Batch Cost
2a)	Silica spheres (0.5um-1.6um), 15ml	315.82	12.63
2b)	Ethanol, semiconductor grade, 40210-2.5L	121.00	24.20

Thermal bath 80degree (300Watt), growth rate 2mm/h
To growth 75mm: Time=37.5h

No	Description	Unit Cost ($)	Batch Cost
2c)	Thermal Bath: Electricity Rate (per kilowatthour)	0.84	9.45

3 Sintering of Silica microspheres

To heat in furnace (1200W) 950C for 3 hours

No	Description	Unit Cost ($)	Batch Cost
3a)	Average Electricity Rate (per kilowatthour)	0.84	3.02

4 Chemical Deposition of ZnO

Batch infiltration, 20g Zn(NO3)2.6H2O, DIW 500ml, 60 degreeC
Thermal bath 60degree (300Watt), 1.5hr
Rinse with DIW (3000ml)
Heat in furnace (1200W), 2hr, 550degreeC

No	Description	Unit Cost ($)	Batch Cost
4a)	Zinc Nitrate Hexahydrate Zn(NO3)2.6H2O, 500g	54.03	2.16
4b)	Deionized water (DIW), 1000 Gallon	15.00	0.01
4c)	Thermal Bath: Electricity Rate (per kilowatthour)	0.84	0.378
4d)	Deionized water (DIW), 1000 Gallon	15.00	0.01
4e)	Furnance : Electricity Rate (per kilowatthour)	0.84	2.016

Repeat step3 for 3 more times (Thermal bath 20hr)

No	Description	Unit Cost ($)	Batch Cost
4a)	Zinc Nitrate Hexahydrate Zn(NO3)2.6H2O, 500g	54.03	6.48
4b)	Deionized water (DIW), 1000 Gallon	15.00	0.03
4c)	Thermal Bath: Electricity Rate (per kilowatthour)	0.84	15.12
4d)	Deionized water (DIW), 1000 Gallon	15.00	0.03
4e)	Furnance : Electricity Rate (per kilowatthour)	0.84	6.048

5 Silica Template Etch

Etch sample in HF (1 wt-%) : 20g HF, 700g DIW

No	Description	Unit Cost ($)	Batch Cost
5a)	Hydrofluoric acid (HF) 35 wt%, 500g (Aldrich)	92.82	3.71
5b)	Deionized water (DIW), 1000 Gallon	15.00	0.01

Total cost per batch run		108.56
Cost per glass slide		10.86
Cost per 1" by 1" sample		3.62

Appendix 3B: Fabrication of Inverted ZnO Opal (equipment cost)

No	Equipment	Retail Cost ($)	Annual Cost (	Cost per batch run ($)
1	Furnace (Fisher 10-550-14, 1200W)	2,021.25	404.25	0.37
2	Thermal Bath (20 liter, Fisher 15-462-20)	1,235.32	247.06	2.82
3	Laboratory consumables			5.00

Note 1
Furnace is forecast to have 5 years lifespan. Annual cost is linear depreciation.
Furnace run time is estimated to be 8hr per batch

Note 2
Thermal Bath is forecasted to have 5 years lifespan. Annual cost is linear depreciation
Thermal bath run time is estimated to be 100hr per batch

Total cost per batch run   8.19

Cost per glass slide   0.82

Cost per 1" by 1" sample   0.27

Reference
Ursaki VV, Tiginyanu IM, Zalamai VV, et al.
Photoluminescence of ZnO layers grown on opals by chemical deposition from zinc nitrate solution
SEMICONDUCTOR SCIENCE AND TECHNOLOGY 19 (7): 851-854 JUL 2004

Photoluminescence and resonant Raman scattering from ZnO-opal **structures**
Author(s): Ursaki VV, Tiginyanu IM, Zalamai VV, Masalov VM, Samarov EN, Emelchenko GA, Briones
Source: JOURNAL OF APPLIED PHYSICS 96 (2): 1001-1006 JUL 15 2004
Document Type: Article

Appendix 4A: Equipment Cost Analysis of a Photolithography System

No	Description	Unit cost ($)	Annual Cost ($)	batch Cost
1	Estimated setup+run time = 45min /batch Photolithography system (0.25µm resolution)	10,000,000.00	1,000,000.00	85.61
2	Estimate 10000 batch for one reticle Reticle	15,000.00	nil	15.00
3	Estimate photoresist, consumables, utility, etching			30.00
	Total cost per batch run			130.61
	Cost per glass slide			13.06
	Cost per 1" by 1" sample			4.35

Note 1
Photolithography system is forecast to have 10 years lifespan. Annual cost is linear depreciation.
Photolithography system setup+run time is estimated to be 45min per batch

http://www.thinfilmmfg.com/subscribers/Subscriber01
/lithocost29Aug01.htm

Appendix 4B: Equipment Cost Analysis of an Electron Beam Lithography System

No	Description	Unit cost ($)	Annual Cost ($)	batch Cost
1	Estimated setup+run time = 3hr /batch Elecrton beam lithography system (0.25µm resolution)	6,000,000.00	600,000.00	205.48
2	Estimate consumables, utility			10.00
	Total cost per batch run			215.48
	Cost per glass slide			21.55
	Cost per 1" by 1" sample			7.18

Note 1
Elecrton beam lithography system is forecast to have 10 years lifespan. Annual cost is linear deprecial
Elecrton beam lithography system setup+run time is estimated to be 3hr per batch

www.njnano.org/resources/fact_sheets/E-Beam_Lithography_20030402.pdf

Reference

[1] B.S. Meyerson, "High Speed Silicon-Germanium Electronics," Scientific American, 270, (3), 42-47, (March 1994).

[2] B.A. Parviz, D. Ryan, G. M. Whitesides, "Using self-assembly for the fabrication of nano-scale electronics and photonic devices", Trans. On Adv. Packaging, Vol. 26, No3. Aug 2003, pp. 233-241.

[3] Glotzer, Solomon, Kotov, Self-Assembly: From Nanoscale to Microscale Colloids, AIChE J., Vol.50, No.12, Dec 2004

[4] Ball, It all falls into place... (News feature), Nature, Vol.413, 18 Oct 2001

[5] M. Boncheva, G. M. Whitesides, "Making things by self-assembly", MRS Bulletin, Vol. 30, Oct 2005.

[6] Intel Silicon Photonic Rsearch, http://www.intel.com/technology/silicon/sp/index.htm

[7] IBM Exploratory Photonic Crystal research, http://www.zurich.ibm.com/st/optics/photonics.html

[8] Photonic Bandgap Link, http://www.pbglink.com/

[9] Science Magazine, New letters, Oct 9 issue.

[10] Online, MIT News Article, Tiny photonic crystals may light way to better optical circuit, October 21, 1998

[11] J D Joannopoulos, R D Meade and J N Winn 1995 Photonic Crystals: Molding the Flow of Light (Princeton University Press)

[12] E. M. Purcell, Spontaneous Emission Probabilities at Radio Frequencies, Phys. Rev. 69, 681, 1946

[13] K. Ohtaka and H. Numata, Multiple scattering effects in photon diffraction for an array of cylindrical dielectrics, Physics Letters A, Vol. 73, pp. 411-413, 1979

[14] E. Yablonovitch, Photonic Crystals: Semiconductors of Light, Sci. American, vol. 285, no. 6, pp. 47-55, December 2001; E. Yablonovitch, Photonic Band-gap Structures, Vol. 10, No. , J. Opt. Soc. Am. B, 1993.

[15] E. Yablonovitch et. al., Inhitbited Spontaneous Emission in Solid-State Physics and Electronics, Phys. Rev. Let. Vol. 58, No 20, pp. 2059, 1987.

[16] E. Yablonovitch et. al., Photonic Band Structure: The Face-Centered-Cubic Case Employing Nanospherical Atoms, Phy. Rev. Let., Vol. 67, No. 17, pp. 2295, 1991

[17] Ho, Chan, Soukoulis, Biswas, Sigalas, Photonic bandgaps in three dimensions: New layer-by-layer periodic structures, Solid State Communications, Vol. 89, No. 5, pp. 413-416, 1994

[18] Noda, Tomoda, Yamamoto, Chutinan, Full Three-Dimensional Photonic Bandgap Crystals at Near-Infrared Wavelengths, Science 2000 Vol. 289 pp. 604-606

[19] Meseguer, Review: Coolidal Crystals as Photonic Crystals, Colloids and Surfaces A: Phyicochem. Eng. Aspects 270-271 (2005) 1-7.

[20] Blanco et al, Large-scale synthesis of a silicon photonic crystal with a complete three-dimensional bandgap near 1.5micrometres, Nature, Vol. 405, pp. 437.

[21] Vlasov, Bo, Sturm, Norris, On-chip natural assembly of silicon photonic bandgap crystals, Nature, Vol. 414, pp. 289.

[22] Ho, Chan, Soukoulis, Existence of a Photonic Gap in Periodic Dielectric Structures, Phy. Rev. Let. Vol. 65, No. 25, pp. 3152, 1990

[23] Florenscio et. al., Nanorobotic Manipulation of Microspheres for On-chip Diamond Architectures, Adv. Mater. 2002, 14, No. 16, pp. 1144

[24] S. Johnson, J. D. Joannopoulos, Three-dimensionally periodic dielectric layered structure with omnidirectional photonic band gap Applied Physics Letters Vol.77, No. 22, 2000

[25] Online, www.pglink.com

[26] Online, http://ab-initio.mit.edu/

[27] Y Xu, G J. Schneider, E D. Wetzel, D W. Prather, Centrifugation and spin-coating method for fabrication of three-dimensional opal and inverse-opal structures as photonic crystal devices, Journal of Microlithography, Microfabrication, and Microsystems, Vol. 3, No. 1, pp. 168–173, January 2004

[28] A A. Zakhidov,* R H Baughman, Z Iqbal, C Cui, I Khayrullin, S O. Dantas, J Marti, V G. Ralchenko, Carbon Structures with Three-Dimensional Periodicity at Optical Wavelengths, Science Vol 282 1998

[29] K. Busch and S. John, "Photonic band gap formation in certain self-organizing systems," Phys. Rev. E 58(3), 3896–3908 (1998) ; B. Gates, S. H. Park, and Y. Xia, "Tuning the photonic bandgap properties of crystalline arrays of polystyrene beads by annealing at elevated temperatures," Adv. Mater.12(9), 653–656 (2000).

[30] Jin et. al., Template-assisted growth, Nano Lett. 2005

[31] Lumsdon, Kaler, Velev, Langmuir 2004, 20, 2108-2116

[32] Y. A. Vlasov, X. Bo, J. C. Sturm, D. J. Norris, On-chip natural assembly of silicon photonic bandgap crystals, Nature, Vol 414, 2001, pp 289.

[33] R Mayoral, J Rquena, J S Moya, C Lopez, A Cintas, H Miquez, F Meseguer, L Vazques, M Holgado, A Blanco, Adv. Mater. 9, 257 (1997)

[34] Goldenberg LM, Wagner J, Stumpe J, et al. Ordered Arrays of large latex particles organized by vertical deposition Langmuir 18 (8): 3319-3323 (2002)

[35] Masse P, Reculusa S, Clays K, Ravaine S , Tailoring planar defect in three-dimensional colloidal crystals, Chem. Phys. Lett. 422 (1-3): 251-255 2006; Palacioslidon E Engineered planar defects embedded in opals, Adv. Mater. 16 , 341, 2004, Chan DLC, Lidorikis E, Joannopoulos JD, Point defect geometries in inverted opal photonic crystals Phy. Rev. E 71 (5), No. 056602 2005

[36] M Allard, E H Sargent, P C Lewis, E Kumacheva, Colloidal Crystals grown on patterned surfaces, Adv. Mater. (2004) 16, No. 15, pp. 1360 ; Winkleman A, Gates BD, McCarty LS, et al. Directed self-assembly of spherical particles on patterned electrodes by an applied electric field , Adv. Mater. 17 (12): 1507-1511 2005

[37] M. Trau, D.A. Saville, I. A. Aksay, Field-Induced layering of colloidal crystals, Science, Vol. 272, pp. 706, 1996. Assembly of Colloidal Crystals at Electrode Interfaces, Langmuir 1997, 13, 6375-6381.

[38] G R Maskaly, R E Garcia, W C Carter, Y M Chiang, Ionic colloidal crystals: ordered, multicomponent structures via controlled heterocoagulation, Phy. Rev. E, 73, 011402, 2006

[39] International Union of Pure and Applied Chemistry, Definitions, Terminology and Symbols in Colloid and Surface Chemistry, http://www.iupac.org/reports/2001/colloid_2001/manual_of_s_and_t/manual_of_s_and_t.html

[40] Foundations of colloid science, Hunter, Robert J. ,Oxford University Press, 2001 ; http://en.wikipedia.org/wiki/Colloid

[41] M Boncheva, G M Whitesides, Making things by self-assembly, MRS Bulletin, Vol 30, pp 736, Oct 2005; Ball, It all falls into place... (News feature), Nature, Vol.413, 18 Oct 2001.

[42] Parviz, Ryan, Whitesides, Using Self-Assembly for the Fabrication of Nano-Scale Electronic and Photonic Devices, IEEE Trans. on Adv. Packing, vol.26, No.3, Aug 2003.

[43] Vlasoc et al., On-chip natural assembly of silicon photonic bandgap crystals, Nature letters, Vol.414, 15 Nov 2001.

[44] Y.N.Xia, B.Gates, Z.Y.Li, Self-assembly approaches to three dimensional photonic crystals, Adv. Mater., vol.13, pp.409-413, 2001.

[45] E.W.Seelig, B.Tang, A.Yamilov, H.Cao, and R.P.H.Chang, Self-assembled 3-D photonic crystals from ZnO colloidal spheres, Mater. Chem. Phys., vol.80, pp.257-263, 2003.

[46] http://news.uns.purdue.edu/UNS/html4ever/010413.Fenniri.naotube.html

[47] S.H.Sun, C.B.Murray, D.Weller, L.Folks and A.Moser, Monodispersive PePt

nanoparticles and ferromagnetic GePt nanocrystal superlatices, Science, vol.287

[48] D J Norris et al., Opaline Photonic Crystals: How does self-assembly work?, Adv. Mater. 2004, 16, No 16, pp 1393

[49] Jiang P, Bertone JF, Hwang KS, V L Colvin, Single-crystal colloidal multilayers of controlled thickness, Chem. Mater.11 (8): 2132-2140 AUG 1999

[50] L M Goldenberg et. al., Ordered arrays of large latex particles organized by vertical deposition, Langmuir (2002), 18, 3319-3323

[51] Yang SM, Ozin GA , Opal chips: vectorial growth of colloidal crystal patterns inside silicon wafers, Chem. Comm. (24): 2507-2508 2000

[52] S Pronk, D Frenkel, J Chem. Phys. 1999, 110, 4589.

[53] P N Pusey, W van Megan, P Bartlett, B J Ackerson, J G Rarity, S M Underwood, Phys. Rev. Lett, 1989, 63, 2753.

[54] C Allain, M Cloitre, M Wafra, Aggregation and Sedimentation in Colloidal Suspensions, Phy. Rev. Lett. Vol 74 No 8 (1995), A van Blaaderen, R Ruel, P Wiltzius, Template-directed colloidal crystallization , Nature 385, 321 - 324 (23 January 1997)

[55] Nagayama, Two-dimensional self-assembly of colloids in thin liquid films, Colloids and Surfaces, 109 (1996) 363-374

[56] D. Deegan et. al., Capillary flow as the cause of ring stains from dried liquid drops , Nature 389, 827 - 829 (23 October 1997); doi:10.1038/39827

[57] Pohl. H. A., Dielectrophoresis, Cambridge University Press, Cambridge, 1978.

[58] P. Richtti, J. Prost, P. Barios, T3:25 PMwo-dimension aggregation and crystallization of a colloidal suspension of latex spheres, J. Physics. Lett. 45, 1137-1143, 1984.

[59] M. Trau, D.A. Saville, I. A. Aksay, Field-Induced layering of colloidal crystals, Science, Vol. 272, pp. 706, 1996. Assembly of Colloidal Crystals at Electrode Interfaces, Langmuir 1997, 13, 6375-6381.

[60] Yeh SR, Seul M, Shraiman BI, Assembly of ordered colloidal aggregates by electric-field-induced fluid flow, NATURE 386 (6620): 57-59, MAR 6 1997

[61] P J Slides, Electrohydrodynamic Particle Aggregation on an Electrode Driven by an Alternating Electric Field Normal to It,Langmuir, 17 (19), 5791 -5800, 2001

[62] Fagan JA, Sides PJ, Prieve DC, Evidence of multiple electrohydrodynamic forces acting on a colloidal particle near an electrode due to an alternating current electric field LANGMUIR 21 (5): 1784-1794 MAR 1 2005

[63] J.O. Bockris and S.U.M. Khan, Surface Electrochemistry: A molecular level approach, Plenum, New York, 1993.

[64] R C Hayward, D A Saville, I A Aksay, Electrophroetic assembly of colloidal crystals with optically tunable micropatterns, Nature, Vol 404, pp. 56, 2000

[65] Choi W M, Park O O, The fabrication of micropatterns of a 2D colloidal assembly by electrophoretic deposition, Nanotechnology 17 (2006) 325-329.

[66] van Blaaderen A, Ruel R, Wiltzius P, Template-directed colloidal crystallization, NATURE 385 6614 (1997)

[67] S.M. Yang, H. Míguez, G.A. Ozin , Opal Circuits of Light - Planarized Microphotonic Crystal Chips, Advanced Functional Materials, Vo 12, (2002) pp. 425-431

[68] E Kumacheva, R K Golding, M Allard, E H Sargent, Colloid crystal growth on mesoscopically patterened surface: Effect of confinement, Adv. Mater. 2002, 14, No 3 221., Winkleman A, Gates BD, McCarty LS, Whitesides GM , Directed self-assembly of spherical particles on patterned electrodes by an applied electric field, Adv. mater 17 (12) 1507-1511 (2005), E. Kim, Y. Xia and G.M. Whitesides, Adv. Mater. 8 (1996), p. 425.

[69] C.-A. Fustin, G. Glasser, H.W. Spiess and U. Jonas, Adv. Mater. 15 (2003), p. 1025, W M Choi and O Ok Park, Micropatterns of colloidal assembly on chemically patterned surface, Vol 277,

Issues 1-3 , (2006) pp. 131-135, C A Fustin et. al., Parameters influencing he templated growth of colloidal crystals on chemically patterned surfaces, langmuir 2004, 20, 91114-9123.

[70] Yan QF, Zhou ZC, Zhao XS, Line defects embedded in three-dimensional photonic crystals, Adv. Mater., 17 (15): 1917, 2005

[71] G R Maskaly, Ph.D. Thesis, Massachusetts Institute of Technology, 2005

[72] F X Redl, K S Cho, C B Murray, S O'Brien, Three-dimensional binary superlattices of magnetic nanocrystals and semiconductor quantum dots., Nature, Vol. 423, 968 (2003)

[73] E V Shvchenko, D V Talapin, N A Kotov, S O"Brien, C B Murray, Structural diversity in binary nanoparticle superlattices, Nature, Vol 439, 55 (2006)

[74] S Simeonov, U Bass and A R McGurn, Physica B 228, 245 (1996)

[75] G R Maskaly, R E Garcia, W C Carter, Y M Chiang, Ionic colloidal crystals : ordered, multicomponent structures via controlled heterocoagulation, Phy. Rev. E., 73, 011402 (2006)

[76] P Bartlett, A I Campbell, Three-dimensional binary superlattices of oppositely charged colloids, PRL 95, 128302 (2005)

[77] M E Lunissen et. al. , Ionic colloidal crystals of oppositely charged particles, Nature, Vol 473, 2005

[78] A P Hynninen, C G Christova, R van Roij, A van Blaaderen, M Dijkstra, Prediction and observation of crystal structures of oppositively charged colloids, PRL, 96 138308 (2006)

[79] M Maldovan, E L Thomas, Diamond-structured photonic crystals, nature materials, Vol 2, 593 (2004)

[80] Rundquist P A, Kesavamoorthy R, Jagannathan, et al., Thermal diffuse scattering from colloidal crystal, J. Chem. Phys., 95 (2): 1249-1257 (1991), Asher et al, US Patent No. 5,281,370 (1994) Method of making solid crystalline narrow band radiation filter. Kamenetzky, E. A., Mangliocco, L. G. & Panzer, H. P., Structure of solidified colloidal array laser filters studied by cryogenic transmission electron microscopy, Science 263, 207–210 (1994)

[81] Pan GS, Kesavamoorthy R, Asher SA, Nanosecond switchable polymerized crystalline colloidal array Bragg diffracting materials, J.Amer. Chem. Soc. 120 (26): 6525-6530, 1998, Weissman JM, Sunkara HB, Tse AS, Asher SA, Thermally switchable periodicities and diffraction from mesoscopically ordered materials, SCIENCE 274 (5289): 959-960 1996

[82] J.D. Joannopoulos, P.R. Villeneuve and S.H. Fan, Photonic crystals: Putting a new twist on light, Nature 387 (1997), p. 830.

[83] C. Lopez, Materials Aspects of Photonic Crystals, Adv. Mater. 15 (2003), p. 1679

[84] R.D. Pradhan, I.I. Tarhan and G.H. Watson, Impurity modes in the optical stop bands of doped colloidal crystals, Phys. Rev. B 54 (1996), p. 13721.

[85] P Masséa, S Reculusaa, K Claysb, S Ravaine, Tailoring planar defect in three-dimensional colloidal crystals, Chemical Physics Letters, Vol 422, Issues 1-3 (2006) Pages 251-255

[86] Y Zhao et. al , The fabrication of photonic band gap materials with a two-dimensional defect, Appl. Phys. Lett, Vo 82, Issue 21 , 26 2003 May, pp 3764-3766

[87] LK Wang, QF Yan, and X. S. Zhao , From Planar Defect in Opal to Planar Defect in Inverse Opal, Langmuir 2006, 22, 3481-3484

[88] E. Palacios-Lidon, J.F. Galisteo-Lopez, B.H. Juarez and C. Lopez, Engineered planar defect embedded in opal, Adv. Mater.16 (2004), p. 341.

[89] Ferrand P, Egen M, Zentel R, Seekamp J, Romanov SG, Torres CMS, Structuring of self-assembled three-dimensional photonic crystals by direct electron-beam lithography, Appl Phys Lett 83 (25): 5289-5291 DEC 22 2003

[90] H S Souzuer, J W Haus, R Ingua, Photonic bands: convergence problems with the plane-wave method, Phys. Rev. B, 45, 13962-13972 (1992)

[91] K Busch, S John. Photonic band gap formation in certain self-organizing systems, Phys. Rev. E, 58, 3896-3908.

[92] Palacios-Lidón, E.; Blanco, A.; Ibisate, M.; Meseguer, F.; López, C.; Sánchez-Dehesa , Optical study of the full photonic band gap in silicon inverse opals, J.. Applied Physics Letters, (2002), Vol. 81 Issue 26, p4925

[93] S Y Lin, J G Fleming, A Three-Dimensional Optical Photonic Crystal, J Lightwave Tech Vol 17, No. 11, (1999)

[94] JFG Lopez et. al., Pro. SPIE Vol 5450, pp498, 2004

[95] Koenderink AF, Vos WL, . Optical properties of real photonic crystals: anomalous diffuse transmission, J Opt Soc Am B-Opt Phys 22 (5): 1075-1084 2005

[96] Allard M, Sargent EH, Appl Phys Lett 85 (24): 5887-5889 DEC 13 2004

[97] Fragility of photonic band gaps in inverse-opal photonic crystals, ZY Li and ZQ Zhang, Phy Rev B Vol 62, No 3 (2000)

[98] Wang ZL, Chan CT, Zhang WY, Chen Z, Ming NB, Sheng P, Optical properties of inverted opal photonic band gap crystals with stacking disorder , Phy Rev E 67 (1) No. 016612 (2003)

[99] L C Chan, E Lidorikis, JD Joannopoulos, Point defect geometries in inverted opal photonic crystals, Phy Rev E 71 056602 (2005)

[100] Miguez H, Tetreault N, Hatton B, Yang SM, Pervoic D, Ozin G, A Chem Comm 2002, 22, 2736.

[101] S Wong, V Kitaev, GA Ozin, Colloidal crystal films: advances in universality and perfection, JACS 2003, 125, 15589-15598.

[102] H Miguez, SM Yang, GA. Ozin, Optical Properties of Colloidal Photonic Crystals Confined in Rectangular Microchannels, 3479 Langmuir 2003, 19, 3479-3485

[103] Maldovan M, Thomas EL, Diamond-structured photonic crystals, Nature Materials 3 (9) 593-600 SEP 2004

[104] F. Meseguer, Colloidal crystal as photonic crystals, Colloids and surfaces, 270-271 (2005), 1-7

[105] F. García-Santamaría, H.T. Miyazaki, A. Urquía, M. Ibisate, M. Belmonte, N. Shinya, F. Meseguer, C. López , Nanorobotic Manipulation of Microspheres for On-Chip Diamond Architectures, Advanced Materials, Volume 14, Issue 16, (2002), pp. 1144-1147

[106] http://photonics.mit.edu/research/

[107] Fasquel S, Melique X, Vanbesien O, Lippens D, Three-dimensional calculation of propagation losses in photonic crystal waveguides, Opt Comm. 246 (1-3): 91-96 2005

[108] Vlasov YA, McNab SJ, Losses in single-mode silicon-on-insulator strip waveguides and bends, OPTICS EXPRESS 12 (8): 1622-1631 APR 19 2004, DK Sparacin, SJ Spector, LC Kimerling, Silicon waveguide sidewall smoothing by wet chemical oxidation, J Lightwave tech, v23 (8), pp 2455-2461 (2005)

[109] S akiyama, MA Popovic, PT Rakich, K Wada, J Michel, HA Haus, EP Ippen, LC Kimerling, J Lightwave Tech, v23(7), pp 2271-2277 (2005)

[110] M. Notomi, A. Shinya, S. Mitsugi, E. Kuramochi, and H-Y. Ryu , Waveguides, resonators and their coupled elements in photonic crystal slabs, Vol. 12, No. 8 Opt Exp (2004) 1551, M Notomi, A Shinya, K Yamada, J Takahashi, C Takahashi, I Yokohama, Structural Tuning of Guiding Modes of Line-Defect Waveguides of Silicon-on-Insulator
Photonic Crystal Slabs, IEEE J Quan Elec Vol. 38, No. 7, 2002

[111] E Chow, S. Y. Lin, J. R. Wendt, S. G. Johnson, J. D. Joannopoulos, Quantitative analysis of bending efficiency in photonic-crystal waveguide bends at l 5 1.55 mm wavelengths, Opt Lett, Vol 26 No 5 (2001)

[112] Fan SH, Villeneuve PR, Joannopoulos JD, Haus HA , Channel drop filters in photonic crystals, Opt Exp 3 (1): 4-11 1998

[113] M. Notomi, A. Shinya, S. Mitsugi, E. Kuramochi, and H-Y. Ryu , Waveguides, resonators and their coupled elements in photonic crystal slabs, Opt ExpVol. 12, No. 8, 1551 (2004)

[114] Hughes S, Extrinsic optical scattering loss in photonic crystal waveguides: Role of fabrication disorder and photon group velocity, Phys Rev Lett 94 : Art. No. 033903 2005

[115] C Sell, C Christensen, J Muehlmeier, G Tuttle, Waveguide networks in three-dimensional layer-by-layer photonic crystals, Appl Phys Lett Vol 84, No 23 (2004)

[116] A Chutinan, S Noda, Highly confined waveguides and waveguide bends in three-dimensional photonic crystal, APL Vol 75, No 24 (1999)

[117] Index of Waveguides in inverted opal photonic crystals, Virginie Lousse, Shanhui Fan, Optics Express (2006) Vol.14, No 2, 866)

[118] Kim HK, Shin J, Fan SH, Digonnet MJF, Kino GS, Source: IEEE J Quant Elec 40 (5): 551-556 2004

[119] Klingshirn et. al., ZnO rediscovered—once again!?, Superl. and Microst. 38 (2005) 209–222

[120] Ma et. al., Effect of the oxygen partial pressure on the properties of ZnO thin films grown by metalorganic vapor phase epitaxy, J. of Crystal Growth 255 (2003) 303–307

[121] J. Singh, Excitation energy transfer processes in condensed matter: Theory and applications, 1994.

[122] Juarez BH, Garcia PD, Golmayo D, et al., ZnO inverse opals by chemical vapor deposition, Adv Mater 17 (22): 2761+ 2005

[123] Scharrer M, Yamilov A, Wu XH, Cao H, Chang RPH, Ultraviolet lasing in high-order bands of three-dimensional ZnO photonic crystals, APL 88 (20): Art. No. 201103 MAY 15 2006

[124] H Kosha et al, Superprism Phenomena in Photonic Crystals: Toward Microscale Lightwave Circuits, APL, 1999, 74, 1370

[125] L Wu, M Mazilu, T Karle, T F Krauss, Superprism phenomena in planar photonic crystals, IEEE J Quan. Elec. Vol 38 No 7 915 (2002)

[126] T Ochiai, J S Dehesa, Superprism effect in-opal based photonic crystals, Phys. Rev. B Vol 64, 245113

[127] B O'Regan, M Gratzel, A low-cost, high-efficiency solar cell based on dye-sensitized colloidal TiO2 films, Nature 353, 737 - 74 (1991)

[128] Mihi A, Miguez H , Origin of light-harvesting enhancement in colloidal-photonic-crystal-based dye-sensitized solar cells, J PHY CHEM B 109 (33): 15968-15976, 2005

[129] Nishimura et al, JACS (2003), 125, 6306 ; C L. Huisman , J Schoonman, A Goossens , The application of inverse titania opals in nanostructured solar cells,Solar Energy Materials and Solar Cells, Vol 85, Issue 1 , (2005), 115-124

[130] Barry RA, Wiltzius P, Humidity-sensing inverse opal hydrogels, LANGMUIR 22 (3): 1369-1374, 2006

[131] Day, J. C.; Robb, I. D. Polymer 1981, 22, 1530-1533

[132] Lee YJ, Pruzinsky SA, Braun PV, Glucose-sensitive inverse opal hydrogels: Analysis of optical diffraction response, Langmuir 20 (8): 3096-3106 APR 13 2004

[133] YJ Lee, PV Braun, Tunable Opal Hydrogen pH Sensors, Adv. Mater. 2003, 15, No 7-8, 2003

[134] Online, Electronics.ca Research Network. Published 01/6/2005.

[135] Communication Technology Roadmap (CTR) 2005 Report. http://mph-roadmap.mit.edu/about_ctr/report2005/

[136] Richard King, Photovoltaics research and development, U.S. Department of Energy

[137] Wired news, http://www.wired.com/news/planet/0,2782,67013,00.html

[138] S Wong, V Kitaev, G A Ozin, Colloidal crystal films: advances in universality and perfection, J Am. Chem. Soc. 2003, 125, 15589-15598

[139] A Blanco et al Large scale synthesis of a silicon photonic crystal with a complete three dimension bandgap near 1.5 um, Nature, Vol 405, 2000, 437

[140] S Hasegawa, S Watanabe, T Inokuma, Y Kurata, Structure and grain boundary defects of recrystallized silicon films prepared from amorphous silicon deposited using disilane, J Appl Phys, 77 (5), 1938 (1995)

[141] H Miguez et al, A new synthetic approach to silicon colloidal photonic crystals with a novel topology and a omni-directional photonic bandgap: micromolding in inverse silica opal (MISO), Adv. Mater.

[142] Wang LK, Yan QF, Zhao XS , From planar defect in opal to planar defect in inverse opal Langmuir 22 (8): 3481-3484 2006

[143] Ursaki VV, Tiginyanu IM, Zalamai VV, et al., Photoluminescence of ZnO layers grown on opals by chemical deposition from zinc nitrate solution, Semi. Sci and Tech 19 (7): 851-854 2004

[144] From the fruitful discussion with Miss The Lay Kuan, MMLab, Nanyang Technological Univeristy

[145] http://www.thinfilmmfg.com/subscribers/Subscriber01/lithocost29Aug01.htm

[146] www.njnano.org/resources/fact_sheets/E-Beam_Lithography_20030402.pdf

[147] Liegl, Summers, Proceeding of SPIE, Vol. 4000, pp 994, (2000)